Journal of Medicinal Chemistry

pubs.acs.org/jmc

Article

Optimization of METTL3 Inhibitors for the Treatment of Solid Tumors and AML

Guillaume Dutheuil,* Killian Oukoloff, François Lenoir, Julien Korac, Mohamed El Bousmaqui, Nicolas Probst, Alexey Lapin, Galina Nakhabina, Nicolas Parmentier, Catherine Sorlet, and Graeme L. Fraser

Cite This: J. Med. Chem. 2026, 69, 9585−9602

Read Online

ACCESS | Metrics & More | Article Recommendations | Supporting Information

ABSTRACT: Further lead optimization of our series of METTL3 inhibitors is disclosed where aggregative replacements of the α-methylpyridone core and 5-dimethylaminopyridin-3-yl-1,2,3-triazole hinge moiety with an oxetan-3-yl-pyridin-3-yl core and 5-cyclopropylpyridin-3-yl-1,3,4-thiadiazol-2-yl hinge moiety, respectively, improved oral bioavailability while decreasing lipophilicity, thereby translating into oral efficacy in mouse tumor models. This research culminates in the discovery of **EP102**, a compound with a clear selectivity profile and a favorable ADME/PK profile in addition to robust efficacy in AML and solid tumor models. **EP102** has entered clinical development for the treatment of advanced solid tumors.

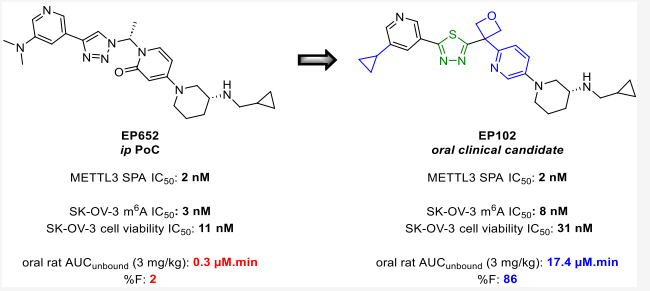

INTRODUCTION

As one of the most abundant epigenetic modifications of RNA, N^6-methyladenosine (m^6A) affects RNA transcription, splicing, stability, and post-transcriptional translation. Methyltransferase-like 3 (METTL3), a key component of the m^6A methyltransferase complex,[1] dynamically regulates target gene expression through m^6A modification. METTL3 has been found to play a critical role in tumorigenesis, tumor growth, metastasis, metabolic reprogramming, immune cell infiltration, and tumor drug resistance. As a result, the development of inhibitors targeted against METTL3 is becoming increasingly popular.[2]

Extensive modeling of existing inhibitors[3] led to the development of a QSAR model, which allowed us to discover hit compound **1** (Figure 1, previously reported). The lead optimization process that delivered the proof-of-concept (PoC) compound **2** (**EP652**) has been disclosed.[4] **EP652** potently inhibits METTL3 and correspondingly decreases cancer cell proliferation across a broad range of *in cellulo* models, encompassing both solid tumors and hematological cancers. However, the *in vivo* efficacy of **EP652** is limited to parenteral dosing. Herein, we report further optimization of this lead series highlighted by improvements in oral bioavailability, as exemplified by oral proof-of-concept compound **3** and further refined in compound **4** (**EP102**). **EP102** demonstrates oral efficacy in various tumor models and an overall profile suitable for development in the treatment of solid tumors.

RESULTS AND DISCUSSION

Improving Oral PK Parameters Starting from *ip* Proof-of-Concept Compound 2 (EP652)

The experience gained through the discovery of PoC compound **2**[4] was applied in the maturation of the lead optimization process toward orally available compounds. Briefly, the bioactivity structure−activity relationship (SAR) previously reported for compound **2** was established through *in vitro* Scintillation Proximity Assay (SPA) and ATPlite assay (antiproliferative effects measured in cell viability assays) across a large panel of cell lines (Calu-6, Caov-3, KG1a, A549, SK-OV-3, FaDu, Kasumi-1, MV-4-11) allowing us to compare our compounds in a cellular setting. Compound **2** is potent in both the SPA primary assay and the ATPlite assays, as well as in an intracellular m^6A inhibition assay (e.g., concentration-dependent inhibition of m^6A on mRNA samples collected from several cell lines *in vitro*) indicative of target engagement. This SAR workflow is further elaborated upon in the current report. Physicochemical characteristics were also monitored constantly (lipophilicity as a main driver through LLE)[5,6] during optimization with a mandate of improving oral PK while maintaining the ADME[7]

Received: February 11, 2026
Revised: March 30, 2026
Accepted: April 8, 2026
Published: April 14, 2026

https://doi.org/10.1021/acs.jmedchem.6c00474
J. Med. Chem. 2026, 69, 9585−9602

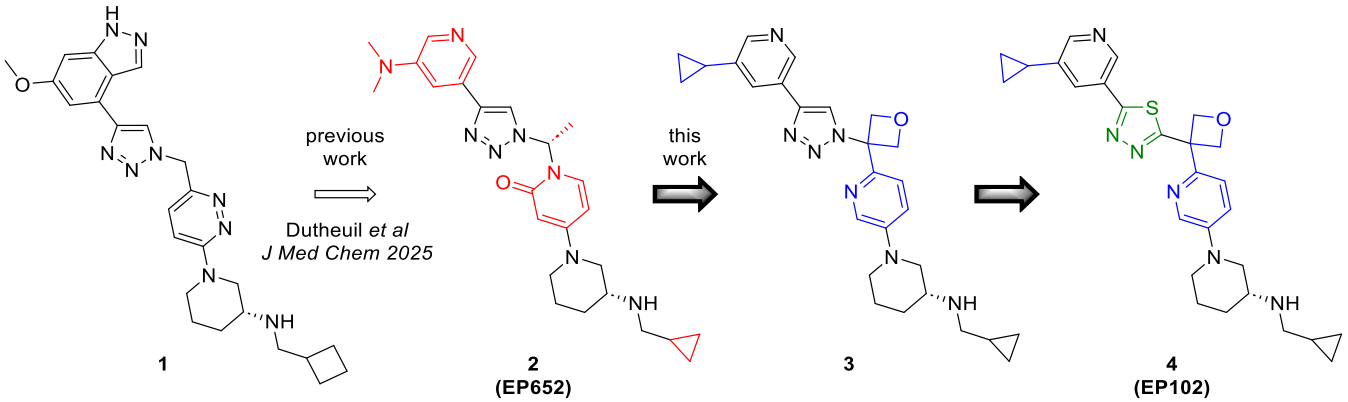

Figure 1. Hit-to-lead progression from hit **1**, to *ip* PoC **2** (**EP652**), to oral PoC **3**, and to clinical candidate **4** (**EP102**).

Table 1. SAR around α-Methylpyridone Core Replacement

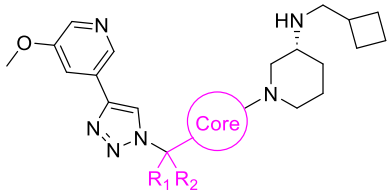

Cpd	Structure	SPA IC_{50} (nM)	Kasumi-1 IC_{50} (nM)	Log $D_{7.4}$	LLE[a]	rfu	*iv* AUC_u[b] (μM.min)	*po* AUC_u[c] (μM.min)
5*	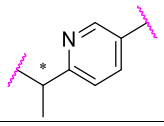	4	2097	1.65	4.03	0.14	10.2	10.9
6*	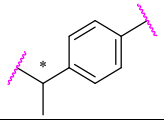	6	1701	2.31	3.46	0.05	3.1	n.d.
7*	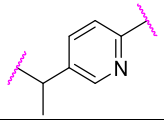	5	3265	1.94	3.55	0.06	2.0	n.d.
8	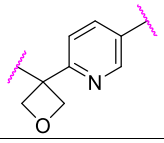	2	236	1.47	5.18	0.16	7.9	12.0
9	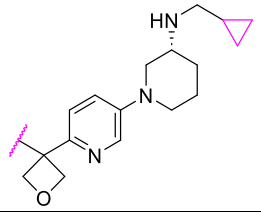	2	270	0.82	5.75	0.28	11.6	11.5

Most potent diastereomer data provided. [a]LLE = pIC_{50} (Kasumi-1) − LogD. [b]AUC_u = rat unbound AUC in *iv* dosing (1 mg/kg/d) = AUC_{total} × rfu. [c]AUC_u = rat unbound AUC in *po* dosing (3 mg/kg/d) = AUC_{total} × rfu. n.d.: not determined.

and efficacy profile. LLE was calculated using pIC_{50} values determined using our cellular assay by ATPlite in Kasumi-1 cells, instead of an assay directly measuring enzymatic inhibition (for example, SPA, even though such data are reported herein), due to the limited dynamic range of the enzymatic inhibition assay to distinguish between highly potent compounds (e.g., compounds with IC_{50} < 3 nM in SPA). In comparison to SPA, the ATPlite assay measuring cell proliferation proved to be a superior assay to distinguish between potent compounds and, furthermore, incorporates any differences in cellular penetration relating to the intracellular targeting required for METTL3 inhibition. The starting point for the current optimization work, compound **2**, has a favorable LLE of 6.28 (Kasumi-1 IC_{50} = 37 nM) and high unbound[8] AUC in *iv* PK in rat and *ip* PK in mouse. However, its poor oral unbound exposure presents a limitation on oral efficacy.

https://doi.org/10.1021/acs.jmedchem.6c00474
J. Med. Chem. 2026, 69, 9585−9602

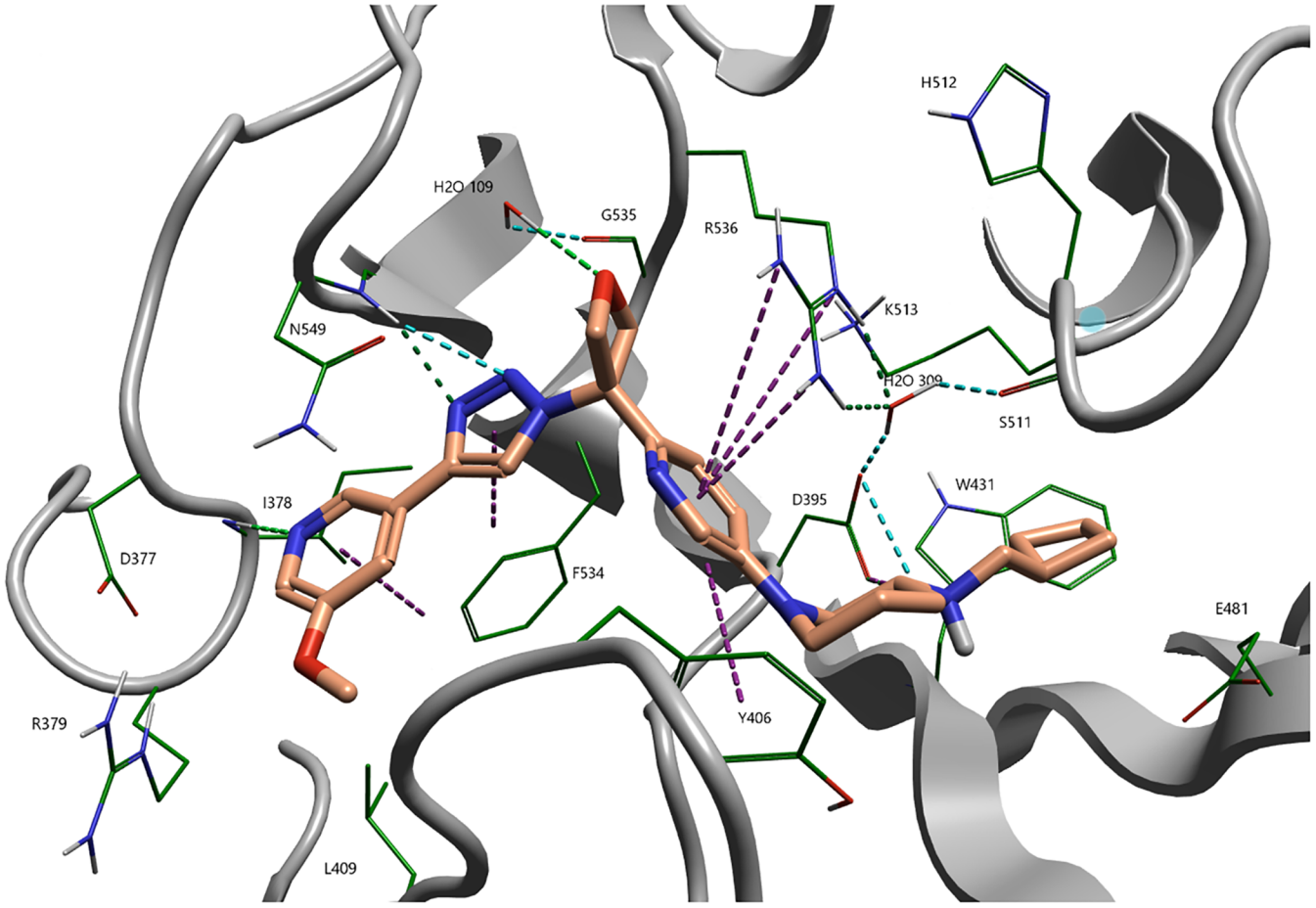

Figure 2. Co-crystal structure of compound **8** (PDB: 9IH5) with a truncated METTL3/14 complex.

In order to improve the metabolic stability of compound **2**, we identified the dimethyl amino moiety on pyridine left-hand side (LHS) and the core pyridone as metabolic soft spots (Figure 1). Accordingly, we returned to an earlier generation of compounds as a new starting point to identify compounds devoid of both of these moieties, whereupon oral unbound PK is significantly improved albeit at the expense of potency. An initial focus is exemplified by compound **5** (Table 1) with methoxypyridine as LHS and pyridin-3-yl core as a new starting point for lead optimization. We had determined that this analogue brings us improved oral unbound PK.[9] Our goal was to improve the potency of this analogue without compromising the oral unbound exposure in the rat.

Based on our prior knowledge from the discovery of compound **2** (**EP652**),[4] we compared best core structures bearing the α-methylation (imparting improved potency and increased free fraction), such as phenyl **6** or pyridin-2-yl **7** (Table 1), and ultimately clearly observed that the pyridin-3-yl core of compound **5** provided a superior scaffold based on its provision of an identical range of potency with improved LogD/LLE and unbound rat *iv* AUC, mostly driven by a higher fraction unbound as measured in rat (rfu). Numerous α-substitutions had already been assessed (mostly with the pyridazine core),[4] and therefore the next step was to test whether the methyl substitution was best. Thus, we again attempted more elaborate substituents that had previously failed in synthesis with both pyridazine and pyridone cores. We targeted moieties that could impart enhanced stability while decreasing global lipophilicity. From these extensive efforts, the introduction of oxetane as *gem*-dimethyl and carbonyl isostere[10] delivered compounds with a favorable overall profile, such as compound **8** (Table 1). In addition to lowering lipophilicity and LogD, which in turn improved the fraction unbound in rat plasma significantly and thereby improved unbound AUC in pharmacokinetic assays, the oxetane moiety also delivered an improvement in potency by nearly one log (compound **5** versus compound **8**). X-ray cocrystallization of compound **8** with the truncated METTL3/14 complex (Figure 2) provided insight into the mechanism by which the oxetane improved potency through enhanced interactions with a network of water molecules; all previously reported interactions[3] remained in place (with Tyr406, Lys513, Asp395, Phe534, and Ile378, PDB code: 9IH5). Addition of the cyclopropyl on the right-hand side of the molecule (a preferred replacement as shown in our previous report)[4] provided compound **9** with further improved LLE, now at 5.75 (against 4.03 for compound **5**, hence nearly 2 log improvement and increased by >0.5 log against compound **8**). Compound **9** demonstrated promising unbound exposure in rat due to significantly improved rfu (0.28), and also showed practicable potency both in *in vitro* SPA assay and *in cellulo* ATPlite assay (Table 1). The latter compound was confirmed to have improved stability in minipig microsomes (half-life of 112 min, improved versus compound **8** (53 min)), while the half-life in rat, dog, and human microsomes was beyond the time limit of the assay (>240 min).

The breakthrough exemplified through compounds **8** and **9** set the core scaffold from which a strategy to further improve potency implicated combination with the best LHS pyridines

https://doi.org/10.1021/acs.jmedchem.6c00474
J. Med. Chem. 2026, 69, 9585−9602

Table 2. SAR around the LHS Pyridine of Compound 9

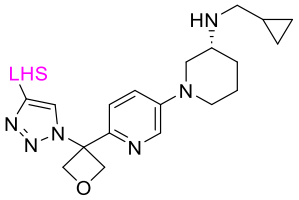

Cpd	LHS	SPA IC_{50} (nM)	Kasumi-1 IC_{50} (nM)	Log $D_{7.4}$	LLE[a]	*iv* AUC_u[b] (μM.min)	*po* AUC_u[c] (μM.min)
10	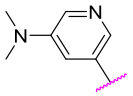	2	62	1.27	5.94	4.0	1.3
11	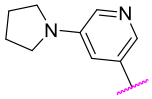	3	18	2.06	5.69	1.4	n.d.
12	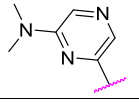	1	122	1.01	5.90	3.0	n.d.
13	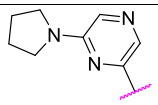	2	81	1.46	5.63	2.9	2.3
14	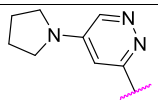	2	162	1.13	5.66	4.1	n.d.
3	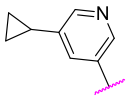	2	113	1.65	5.32	4.6	4.3
15	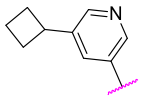	2	131	2.30	4.58	2.4	n.d.
16	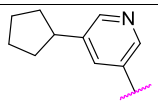	2	137	2.74	4.12	1.5	n.d.
17	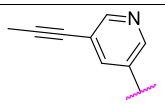	2	215	1.82	4.85	7.7	n.d.
18	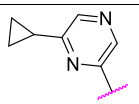	4	406	1.34	5.05	4.0	n.d.
19	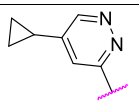	1	716	0.89	5.26	n.d.	n.d.

[a]LLE = pIC_{50} (Kasumi-1) − LogD. [b]AUC_u = rat unbound AUC in *iv* dosing (1 mg/kg/d) = AUC_{total} × rfu. [c]AUC_u = rat unbound AUC in *po* dosing (3 mg/kg/d) = AUC_{total} × rfu. n.d.: not determined.

and pyrazines/pyridazines variants, as discovered earlier ("hinge" moiety).[4] This SAR was extensively explored and is summarized by compounds **10**−**14** (Table 2). Notably, the anticipated potency gain delivered by the aminopyridine (compounds **10**, **11**) or pyrazine (compounds **12** and **13**), and pyridazine (compound **14**) LHS was offset by the deterioration of PK parameters. Therefore, we turned our attention toward small electron-rich alkyl LHS substituents and confirmed that this strategy indeed allowed us to make very potent compounds based on testing *in cellulo* as exemplified in the Kasumi-1 assay (compound **3** and compounds **15**−**17**). It was observed that the electron-rich cyclopropyl of compound **3** was (again) the best substituent (compare against compounds **15**−**17**, Table 2), affording a very potent compound, while maintaining LogD in the lower range and providing very high unbound AUC in rat both *iv* and *po* (>3-fold higher than the corresponding dimethyl amino **10**). In addition, cyclopropyl-substituted pyrazine **18** and pyridazine **19** variants were synthesized, but both analogs were disappointing in cellular inhibition in Kasumi-1 cells and further exhibited poor unbound AUC, thereby providing additional evidence that the pyridin-3-yl is the LHS heterocycle of choice. Co-crystals of the truncated

https://doi.org/10.1021/acs.jmedchem.6c00474
J. Med. Chem. 2026, 69, 9585−9602

METTL3−14 complex with compounds **13** and **3** were obtained, where both compounds exhibited similar binding interactions as previously shown with compound **8** (Figure 2), but with the addition of an interaction of the lipophilic moiety (pyrrolidine of compound **13**, or cyclopropyl of compound **3**) with Leu409 (PDB: 9Q89 and 9Q8A).

Finally, the exploration of the oxetane isosteres was completed by synthesizing the carbon (difluoro-cyclobutyl) and nitrogen (NH and NMe azetidines) versions of oxetane **3** and testing in the Kasumi-1 assay to thereby provide further confirmation that these analogs (not shown) were significatively less potent, consistent with the increased lipophilicity for the cyclobutyl analogue, while the poor potency of the azetidines *in cellulo* was attributed to decreased permeability.

Confirmation of Efficacy with Oral Proof-of-Concept Compound 3

As a consequence of compound **3** demonstrating a suitable pharmacokinetic profile (Table 2) and promising *in vitro* efficacy (as measured in the Kasumi-1 cell line), compound **3** was advanced into efficacy testing across a broad panel of cancer cell lines *in vitro* (Table 3). To confirm the effect observed on cell proliferation, Calu-6 was selected as a representative cell line to measure the inhibition of intracellular m^6A, the latter used as a marker of target engagement.

Table 3. Efficacy Data *In Vitro* of Compound 3

compound 3	
SPA IC_{50} (nM)	2
Cell viability (ATPLite, IC_{50} (nM), 72 h)	
Kasumi-1	113
MV-4-11	1084
Calu-6	86
A549	559
FaDu	200
SK-OV-3	38
Caov-3	76
intracellular m^6A IC_{50} (nM) Calu-6	22

Following the confirmation of broader efficacy *in vitro* of compound **3**, its oral efficacy was assessed in a disseminated xenograft model of AML by intravenous injection of MV-4-11 cells (AML, MV-4-11-Luc-mCh-Puro CDX Model, implant of 2×10^6 cells) in female NSG mice. Compound **3** dosed by the oral route at a single concentration in this proof-of-concept study (100 mg/kg, *po*, QD for 22 days) was initiated at 5 days postimplant versus vehicle-treated control. The main study arms were subjected to imaging (bioluminescence imaging: BLI) once weekly up to day 27 (22 days of treatment). Compound **3** showed strong tumor growth inhibition (Supporting Information Figure S7) as measured by in-life imaging. Consistent with the in-life imaging results, flow cytometric analysis of bone marrow from mice (N = 5/group) terminated on day 27 revealed a selective reduction of hCD45$^+$ versus mCD45$^+$ cells, indicative of inhibited AML tumor growth (Supporting Information Figure S7).

From Oral Proof-of-Concept Compound 3 to Clinical Candidate 4 (EP102)

The demonstration that oral efficacy was achieved with compound **3** validated the continued optimization of this lead series with the mandate to improve potency while maintaining oral bioavailability. Moreover, in consideration of process development and scale-ups, removal of the 1,2,3-triazole moiety was considered to be an additional potential benefit to the overall project. Safety evaluation performed on the corresponding possible azide intermediates identified potential hazardous characteristics upon heating. Replacement of this 5-membered heterocycle in our earlier α-methylpyridone series (e.g., compound **2**) was previously reported[4] with few isosteres demonstrating any potential, with the exceptions being the imidazole, pyrazole, and thiadiazole. Based on this data set, we first used compound **13** as a template (parallel investigation as in Table 2), and we were able to access imidazole variant **20**, thiadiazole **21**, and amide **22** (Table 4). Unfortunately, synthesis of the pyrazole-oxetane-pyridine sequence was unsuccessful, as we were unable to develop a coupling reaction to assemble aryl-substituted or protected 1*H*-pyrazol-4-yl and oxetan-3-ylpyridine (successful pathways developed toward analogs are described below in Schemes 2 to 7). Further attempts to access this sequence through late oxetane formation from diol were not easier to carry out in our hands.

In comparison with triazole **13**, imidazole **20** exhibited inferior oral unbound AUC albeit with similar potency, while thiadiazole **21** afforded a 3-fold more potent compound in ATPlite assay (Kasumi-1 cell line), alongside a greater than 2-fold improved *iv* unbound AUC. However, the oral unbound AUC for compound **21** was low, as attributed to the presence of the amino-pyrazine as LHS, consistent with the observation reported for the SAR presented in Table 2. Amide **22** exhibited significantly improved oral unbound AUC, but at the expense of *in cellulo* potency. In pursuit of ameliorated oral PK parameters versus compound **21**, we completed the synthesis of 5-cyclopropyl-pyridin-3-yl LHS variant **4** (identical LHS as for compound **3**) that delivered superior potency than compound **3** (as expected) in addition to an improved oral unbound AUC (>4-fold versus triazole **3**). The oxadiazole analogue **23** was also made, and this compound reproduced the poor profile reported previously for oxygen-containing heterocycles.

X-ray crystallization analysis of the binding of compound **4** to the truncated METTL3/14 complex (Figure 3) recapitulated all the well-described interactions in the literature[3] (with Tyr406, Lys513, Asp395, Phe534, and Ile378 such as PDB: 7ACD, 7O2I), including the interactions disclosed for our own analogues as published earlier[4a] (PDB: 9G4U, 9G4S, and 9G4W).[11] Additional interactions between the oxetane and water molecules were clearly visible (similar to that shown with compound **3**, Figure 2).

EP102 Selection Validation

Compound **4** (**EP102**) was nominated as a development candidate based on its overall profile. **EP102** potently inhibits METTL3 as measured in enzymatic inhibition assays by SPA (Table 5). In ATPlite-based cell viability assays, **EP102** showed nanomolar potency across a broad panel of cancer cell lines (Kasumi-1 and MV-4-11 (AML), Calu-6 and A549 (lung), FaDu (head and neck), and Caov-3 and SK-OV-3 (ovarian)). Inhibition of intracellular m^6A, used as a marker of target engagement, was also measured in many of these cell lines, with potent m^6A inhibition corresponding to the effects observed on cell proliferation.

The cell-based efficacy profile of **EP102** justified its selection for extensive profiling (ADME, selectivity assessment, preliminary evaluation of toxicity, and full PK assessment). The ADME profile is summarized in Table 6. **EP102** exhibited suitable plasma protein binding (PPB) values (high fractions unbound)

https://doi.org/10.1021/acs.jmedchem.6c00474
J. Med. Chem. 2026, 69, 9585−9602

Table 4. SAR around Triazole Replacement of Compounds 3 and 14

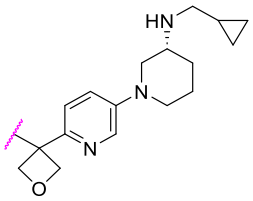

Cpd	Structure	SPA IC_{50} (nM)	Kasumi-1 IC_{50} (nM)	Log $D_{7.4}$	LLE[a]	*iv* AUC_u[b] (μM.min)	*po* AUC_u[c] (μM.min)
20	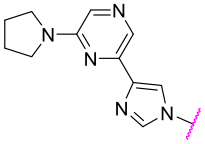	1	71	1.44	5.71	1.0	0.5
21	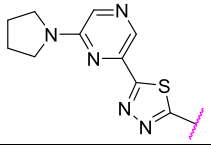	1	27	2.28	5.30	7.6	0.8
22	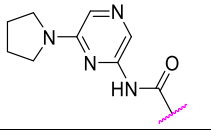	2	183	1.23	5.56	4.9	5.8
4	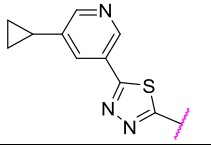	2	61	1.74	5.46	7.2	17.4
23	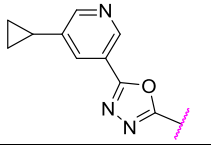	57	4841	1.04	4.28	n.d.	n.d.

[a]LLE = pIC_{50} (Kasumi-1) − LogD. [b]AUC_u = rat unbound AUC in *iv* dosing (1 mg/kg/d) = AUC_{total} × rfu. [c]AUC_u = rat unbound AUC in *po* dosing (3 mg/kg/d) = AUC_{total} × rfu. n.d.: not determined.

in all species, predictive of high unbound AUCs in pharmacokinetic evaluations. Nonselective cytotoxicity was assessed, and **EP102** did not affect HepG2 viability at test concentrations up to 50 μM nor did **EP102** affect viability in primary human hepatocytes at a test concentration of 10 μM; these were the highest test concentrations tested in each assay, respectively. **EP102** metabolism in microsomes and hepatocytes was studied in rat, minipig, and human and revealed that compound stability translated well across species with adequate half-life projections in all cases. Extensive CYP profiling was performed, and significant inhibition was not observed at a test concentration of 10 μM at the 10 main CYPs, with the exception being at CYP3A4 (IC_{50} = 0.9 μM). Cardiovascular toxicity was preliminarily assessed by electrophysiological evaluation of hERG inhibition with an IC_{50} of 17 μM, affording a comfortable safety margin against projected efficacious plasma concentrations in a clinical setting.

EP102, tested at a single concentration of 10 μM, selectively inhibited METTL3/14 among a panel of 40 methyl transferases (Figure 4, and complete details in Supporting Information), additionally complemented by FTO (the main m^6A demethylase). In addition, standard safety screening of **EP102** tested at 10 μM against a large panel of targets (87 targets, including GPCRs, ion channels, kinases, transporters, etc.) did not reveal any major off-target selectivity issues.

The pharmacokinetic profile of **EP102** (Figure 5) was determined in mouse, rat, and minipig. Intravenous (*iv*) and oral (*po*) PK parameters in rat revealed moderate clearance (Cl at 50.1 mL/min/kg, hence unbound Cl at 310 mL/min/kg), good exposure (AUCs unbound in Table 4), and oral bioavailability (F) of 86% (Figure 5A). Absence of drug accumulation in rat after 5 days of administration with **EP102** was verified (7.5 mg/kg/d, QD, orally, Supporting Information Figure S5). Dose-dependent exposure was verified in repeat-dose oral PK experiments in mouse, from 10 to 30 mg/kg/d (QD) sampled on day 5 of chronic dosing with exposures of AUC_u = 57.9 and 223.8 μM·min respectively with no appearance of drug accumulation (Supporting Information Figure S6), a pharmacokinetic profile thereby supporting repeated, oral dosing in mouse cancer models (*vide infra*). **EP102** also demonstrated significant exposure in single dose oral PK in minipig (Figure 5B), with unbound AUC very similar to that of rat (comparing both at 3 mg/kg). There were no signs of gender differences affecting PK parameters across species, as shown for the minipig and also determined in rat (data not shown; PK in male rat below).

https://doi.org/10.1021/acs.jmedchem.6c00474
J. Med. Chem. 2026, 69, 9585−9602

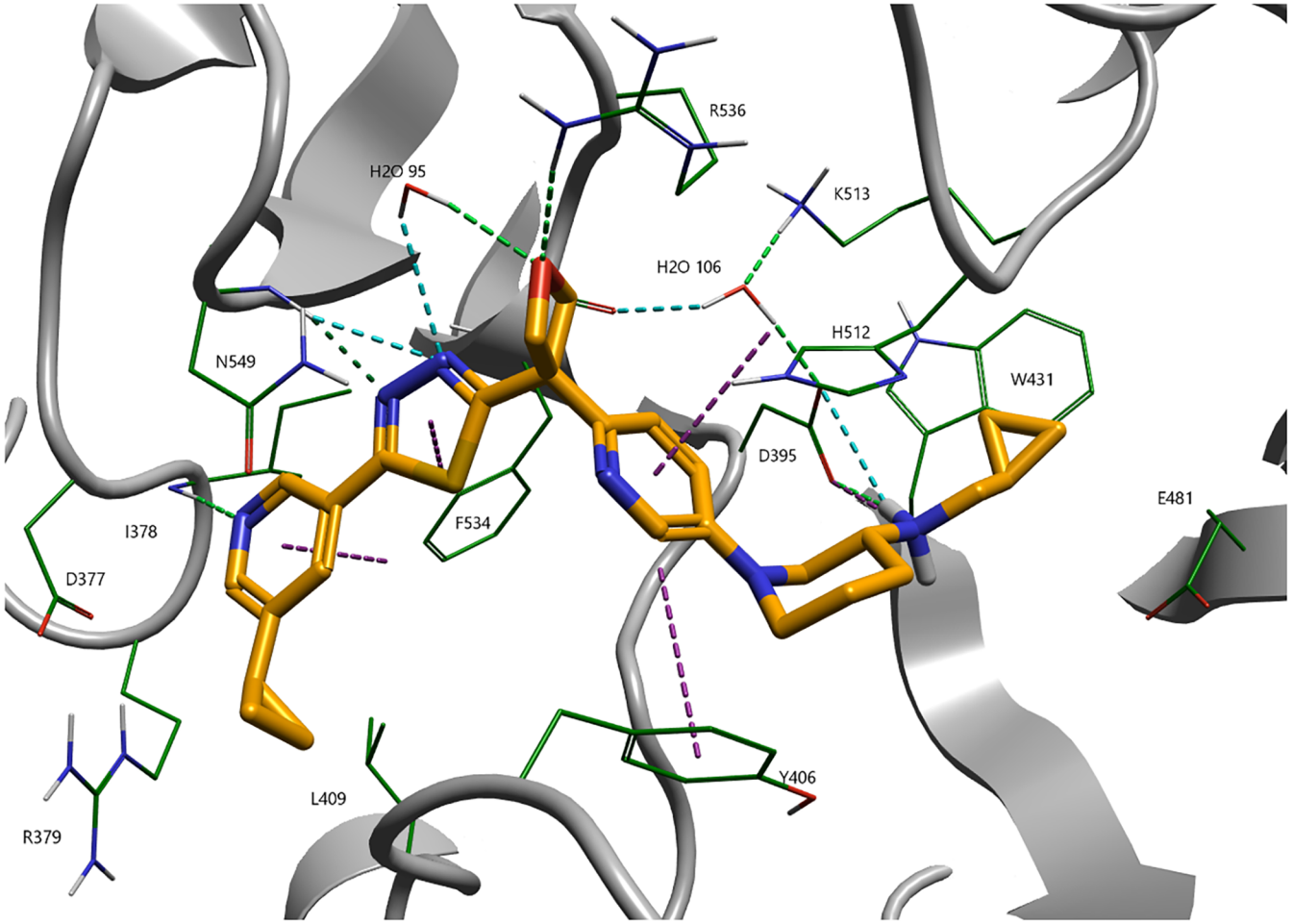

Figure 3. Co-crystal structure of compound **4** (**EP102**) (PDB: 9Q8G) with the truncated METTL3/14 complex.

Table 5. Efficacy Data *In Vitro* of Compound 4 (EP102)[a]

	4 (EP102)	
	2	
SPA IC_{50} (nM)	cell viability (APTLite, IC_{50} (nM), 72 h):	intracellular m^6A (IC_{50} (nM)):
Kasumi-1	61	8
MV-4-11	200	15
Calu-6	36	19
A549	180	17
FaDu	225	16
SK-OV-3	31	6
Caov-3	56	n.d.

[a]n.d.: not determined.

Table 6. EP102 ADME and PK Profile

ADME profiling assay	EP102
rfu	0.16
mfu	0.16
mpfu	0.34
hfu	0.10
HepG2 viability at 50 μM	94%
RLM $T_{1/2}$	149 min
MpLM $T_{1/2}$	44 min
HLM $T_{1/2}$	53 min
rat hepatocytes $T_{1/2}$	>240 min
minipig hepatocytes $T_{1/2}$	70 min
human hepatocytes $T_{1/2}$	65 min
CYPs inhibition (IC_{50}, μM):	
1A2/2C19/2C9/2D6/3A4	>100/70/94/13/0.9
2A6/2B6/2C8/3A5/2E1	>30/>30/>30/16/>30
*h*ERG binding IC_{50}	17 μM

In Vivo Evaluation of EP102, m^6A Target Engagement Biomarker

Following oral administration of **EP102** in rats, evaluation of the PBMCs from these animals revealed a concentration-dependent decrease in mRNA m^6A levels, indicating *in vivo* target engagement relative to vehicle-treated controls (Figure 6A). **EP102** demonstrated a dose-dependent inhibition of m^6A up to a maximum reduction (79%)[12] following a single dose of 3 mg/kg. The time-course for recovery of m^6A was also measured following a dose of 3 mg/kg (Figure 6B) with an approximate recovery up to 70% of baseline levels at 24 h postdosing and a full recovery to baseline levels at 48 h. Notably, the dynamics of m^6A turnover lag the pharmacokinetic exposure of **EP102** as the pharmacokinetic analysis reveals that the compound clears over a 24 h period in rat at the same dose (3 mg/kg, oral; data in Figure 5A). Overall, the dynamics of m^6A recovery, rather than the pharmacokinetic profile of **EP102**, is suggestive that dosing every other day may be sufficient to attain an optimal therapeutic response.

https://doi.org/10.1021/acs.jmedchem.6c00474
J. Med. Chem. 2026, 69, 9585−9602

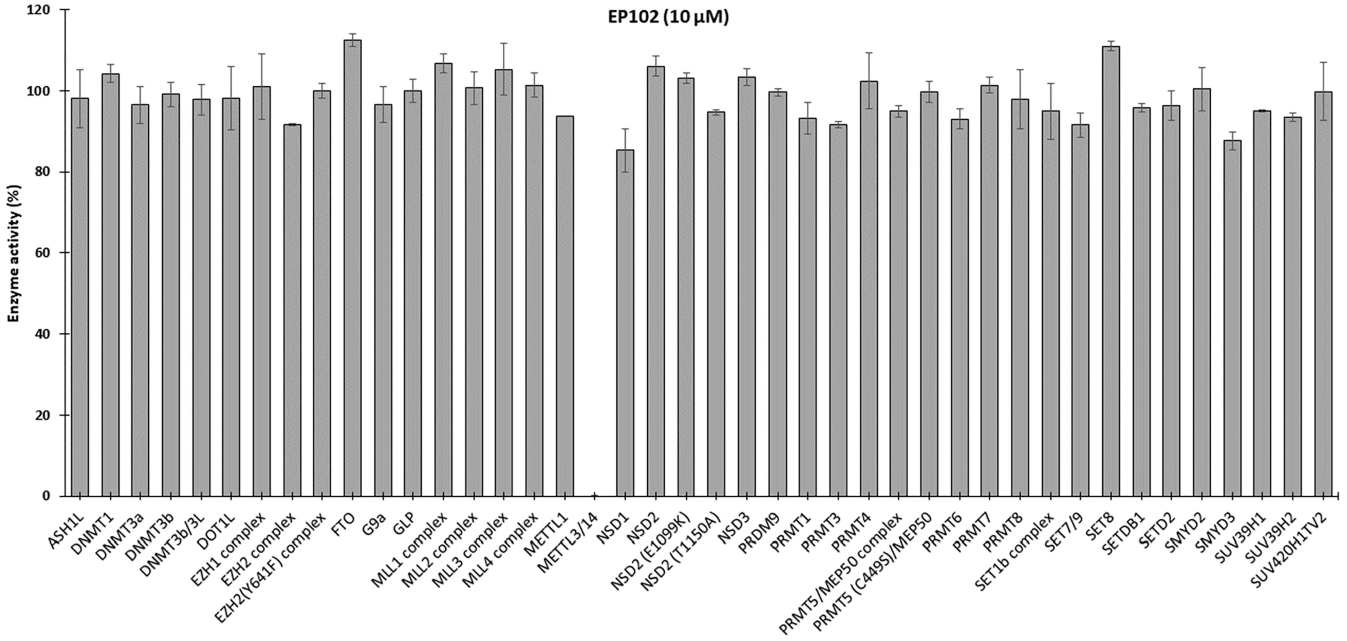

Figure 4. EP102 inhibition (duplicates) of 40 methyl transferases and FTO demethylase at 10 μM.

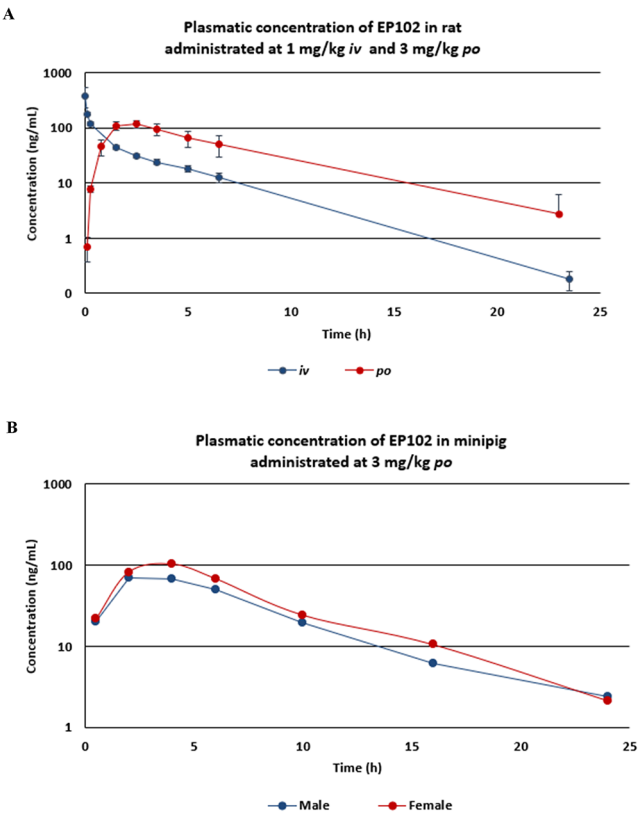

Figure 5. Pharmacokinetics of **EP102** in rat (A) following a single administration at 1 mg/kg *iv*, or 3 mg/kg *po* (plasma concentration vs time), and in minipig (B) following a single administration at 3 mg/kg, *po* (plasma concentration vs time).

In Vivo Evaluation of EP102 in Mouse Tumor Models

EP102 was evaluated in the same disseminated AML xenograft model (MV-4-11-Luc-mCh-Puro CDX model) previously employed for our proof-of-concept compound **2**[4] (intraperitoneal dosing) and as mentioned earlier with compound **3** (oral dosing, Supporting Information Figure S7). Mice were treated with either daily dosing of **EP102** (20 mg/kg, *po*, QD), or 3 doses per week (47 mg/kg, *po*, TIW) for 4 weeks; notably, the weekly compound consumption is the same in both cases where the frequency of dosing is compared to evaluate whether efficacy best matches pharmacokinetic exposure or the dynamics of m^{6}A turnover. Both dose regimens of **EP102** demonstrated clear improvement to restrict the spread of cancer as shown by tumor imaging (Figure 7A) and FACS analysis of *h*CD45$^+$ cells in bone marrow (Figure 7B); no concomitant depletion was observed for *m*CD45+ cells (not shown). The TIW dose regimen showed superior efficacy over QD dosing. Treatment with **EP102** was well-tolerated over the course of the experiment, and body weights of treated mice were stable up to study termination.

Compound **2** was previously reported to be effective in the SK-OV-3 model of ovarian cancer.[4] Ovarian cancer may be of particular interest for treatment with a METTL3 inhibitor based on our observation that METTL3 is coamplified with PARP2[13] (Figure 8A), where PARP2 is known to be a particularly important driver of this tumor type.[14] Thus, **EP102** was tested in the SK-OV-3-Luc model (female Balb/c mice, intraovarian implant) on the same dose regimen proven to be most effective in the AML model (47 mg/kg, *po*, TIW). In response to **EP102** treatment, > 90% tumor growth inhibition (TGI, measured by bioluminescence) was observed relative to the vehicle group over the 32-day treatment period, the latest time point with a full complement of surviving mice in the vehicle group (Figure 8B,C). Similarly robust efficacy was observed in response to the standard-of-care PARP inhibitor olaparib (50 mg/kg, *po*, QD, positive control), although only **EP102** treatment appeared to reduce metastasis based upon tumor flux measured in the intestines (Figure 8D). Body weights were stable in response to **EP102** or olaparib treatment (Figure 8E), and there were no observations of macroscopic adverse events.

In summary, this report describes the optimization from *ip* proof-of-concept compound **2** to deliver oral proof-of-concept compound **3** (Figure 1) via modification of identified metabolic

https://doi.org/10.1021/acs.jmedchem.6c00474
J. Med. Chem. 2026, 69, 9585−9602

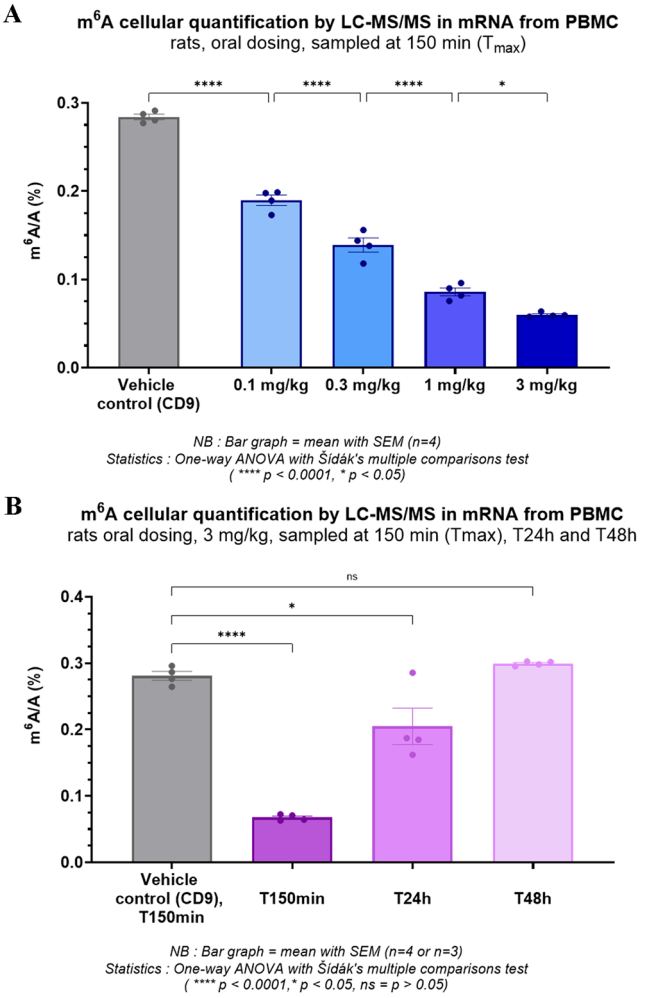

Figure 6. m^{6}A cellular quantification in mRNA from PBMC after oral treatment with **EP102**. (A) 0.1−3.0 mg/kg treatment (single dose) with **EP102** with maximum inhibition shown at 3 mg/kg. (B) Single dose at 3 mg/kg and m^{6}A level recovery after 24 and 48 h postdosing.

soft spots. Compound **3** afforded the first demonstration of oral efficacy in a mouse model of AML. Further optimization allowed us to identify **EP102** as our development candidate. Its nomination was based on its superior efficacy across a large panel of cell lines *in vitro* and *in cellulo* (Table 5) in correspondence with m^{6}A intracellular inhibition, a target engagement biomarker established in the same panel of cell lines. **EP102** also demonstrated a suitable ADME profile (Table 6), selectivity profile (Figure 4), and pharmacokinetic profile (Figure 5) to support its selection as a development candidate. Furthermore, m^{6}A cellular quantification in mRNA extracted from PMBC, after oral dosing in rat, confirmed dose-dependent target engagement *in vivo* (Figure 6) and was informative with regard to the dynamics of m^{6}A turnover, suggestive of a TIW dose regimen in mouse cancer models. **EP102** demonstrated clear inhibition of tumor growth in AML (Figure 7) and ovarian cancer (Figure 8) models.

Chemistry

The synthesis of compound **5** was already described.[4,9] Compounds **6** and **7** were prepared by using analogous pathways (Scheme 1). 4-Bromobenzaldehyde **24** was reacted, using the Buchwald−Hartwig[15] reaction to introduce the protected chiral piperidine, followed by methylation of the corresponding aldehyde to provide intermediate **25**. Introduction of azide was performed with DPPA,[16] followed by click[17] chemistry with 3-ethynyl-5-methoxypyridine to afford **26**. Simple Boc deprotection yielded **6**, and both diastereomers were separated by chiral preparative HPLC. For compound **7**, the sequence was inverted and LHS triazole was introduced before piperidine RHS. Methyl ketone of **27** was reduced into alcohol, before mesylation and substitution with azide (see the Supporting Information for full details) to deliver intermediate **28**. Then, click reaction allowed building of the triazole moiety of **29** and Buchwald−Hartwig coupling completed the access to **30**. Final deprotection delivered compound **7**, which was purified to pure diastereomers by chiral preparative HPLC as well.

Oxetane-containing compounds **3** and **8** to **16** were prepared by the addition of lithiated 5-bromo-2-iodopyridine **31** onto commercially available *tert*-butyl sulfinamide **32** (Scheme 2). Intermediate **33** was then reacted in Buchwald−Hartwig coupling as described above to provide **34** or **35**. Iodine-mediated deprotection of the sulfinyl amines afforded corresponding amines **36** and **37**, which were converted into desired azides **38** and **39** using diazo transfer reagent 2-azido-1,3-dimethylimidazolinium hexafluorophosphate (ADMP).[18] Click reactions using alkynes of interest (full synthetic details in Supporting Information) were carried out using either TMS-protected alkynes and CuF_2 sup-stoichiometrically[19] or using deprotected alkynes and catalytic CuI. Final Boc deprotection of **40** and **41** (**A to I**) afforded the desired compounds.

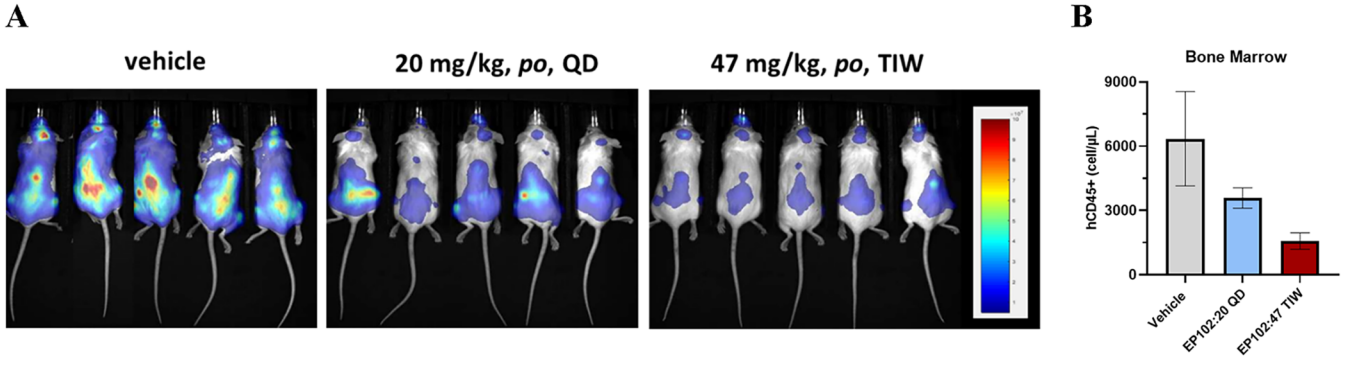

Figure 7. (A) Bioluminescence imaging (day 26, postimplant) of MV-4-11 AML cells, vehicle versus **EP102** treated (20 mg/kg, *po*, QD and 47 mg/kg, *po*, TIW). Color scale: from blue 5×10^6 photons/sec/cm^2/sr to red 1×10^8 photons/sec/cm^2/sr. (B) Flow cytometry at study termination shows **EP102** treatment selectively decreases *h*CD45$^+$ cells on bone marrow ($p < 0.05$).

https://doi.org/10.1021/acs.jmedchem.6c00474
J. Med. Chem. 2026, 69, 9585−9602

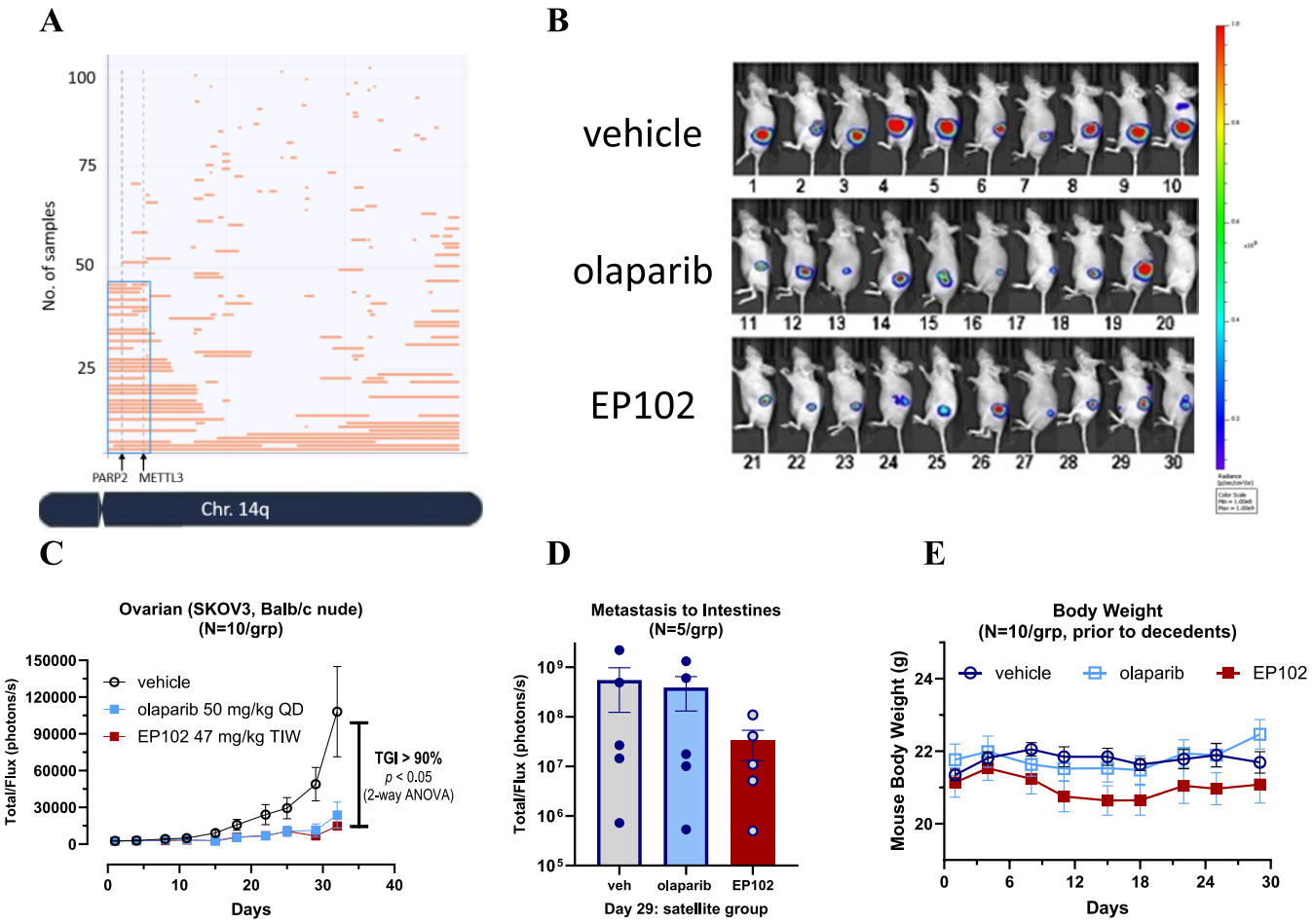

Figure 8. (A) Span of amplifications affecting the q-arm of chromosome 14 in ovarian carcinoma samples. The horizontal lines indicate the amplified region. PARP2 and METTL3 are marked with black arrow. Gene block coamplified with METTL3 and PARP2 is marked with the blue box. (B) Imaging of tumor growth in mice on day 29. (C) Tumor growth curve was measured by total flux. (D) Tumor metastases to the intestines. (E) Body weight measurements were performed prior to the emergence of decedents.

Scheme 1. Preparation of Compounds 6 and 7[a]

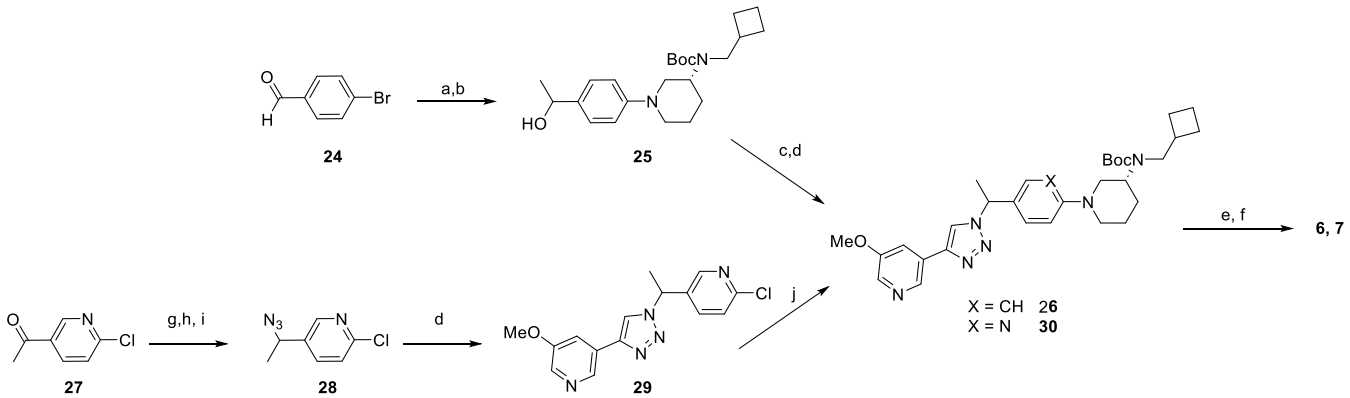

[a]Reagents and conditions: (a) *tert*-butyl (*R*)-(cyclobutylmethyl)(piperidin-3-yl)carbamate, $Pd(OAc)_2$, *rac*-BINAP, Cs_2CO_3, toluene, 100 °C, 17 h, 71%; (b) MeMgCl, THF, −78 °C, 1 h, 96%; (c) DPPA, DBU, toluene, 0 °C to rt, 3 h, 41%; (d) 3-ethynyl-5-methoxypyridine, CuI, DMF, rt, 15 h, 60−68%; (e) HCl 4 M in 1,4-dioxane, MeOH, rt, 16 h, 71−100%; (f) chiral preparative HPLC, 46−47%; (g) $NaBH_4$, MeOH, 0 °C, 20 min, 93%; (h) MsCl, NEt_3, DCM, 0 °C to rt, 1 h, 95%; (i) NaN_3, DMF, 70 °C, 1 h, 96%; (j) *tert*-butyl (*R*)-(cyclobutylmethyl)(piperidin-3-yl)carbamate, NEt_3, NMP, 120 °C, 16 h, 15%.

To access the oxetane-containing analogues **17** to **19**, we used 3-oxetanone as an oxetane electrophile (Scheme 3) and assembled the triazole moiety first before introducing the chiral piperidine. Accordingly, **42** was added to oxetanone after halogen-lithium exchange. Alcohol **43** was transformed into azide **45** as shown in Scheme 1. Next, click reaction via either sup-stoichiometric or catalytic methods afforded the desired intermediates triazole **46** (**A-C**). Those were reacted in a Pd-

https://doi.org/10.1021/acs.jmedchem.6c00474
J. Med. Chem. 2026, 69, 9585−9602

Scheme 2. Preparation of Compounds 3 and 8−16[a]

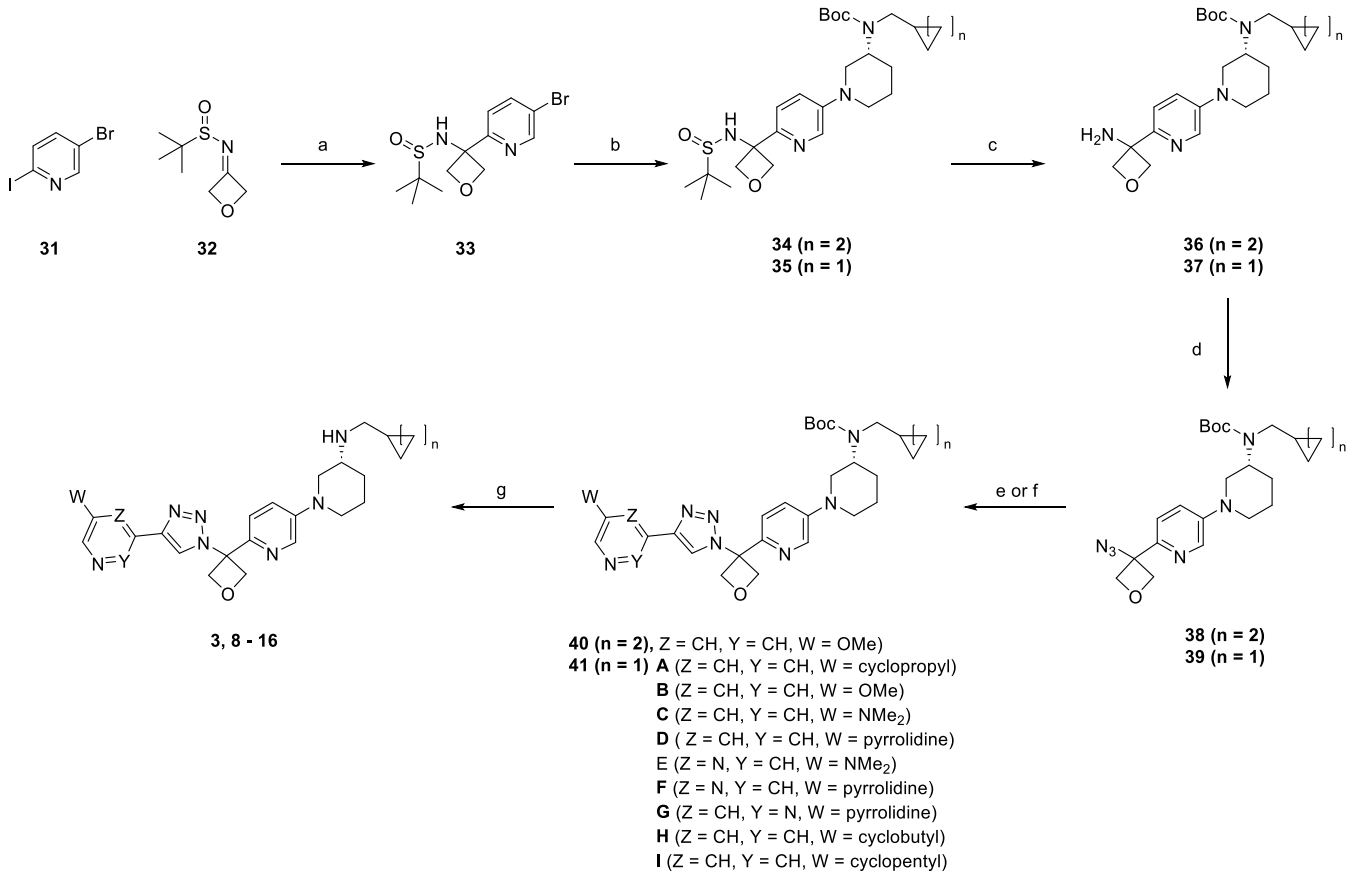

[a]Reagents and conditions: (a) *n*BuLi, THF, −78 °C, 1.5 h, 53%; (b) *tert*-butyl (*R*)-(cyclobutylmethyl)(piperidin-3-yl)carbamate or *tert*-butyl (*R*)-(cyclopropylmethyl)(piperidin-3-yl)carbamate, RuPhos Pd G4, Cs_2CO_3, *t*-AmylOH, 85 °C, 17 h, 38−67%; (c) I_2, THF, 55 °C, 1.5 h, 80−99%; (d) ADMP, Et_2NH, MeCN, 30 °C, 1.25 h, 56−79%; (e) TMS-alkyne, CuF_2, DMF, 60 °C, 16 h, 41−96%; (f) alkyne, CuI, DMF, rt, 5 h, 70−96%; (g) TFA, DCM, rt, 20 min, 57−96%.

Scheme 3. Preparation of Compounds 17−19[a]

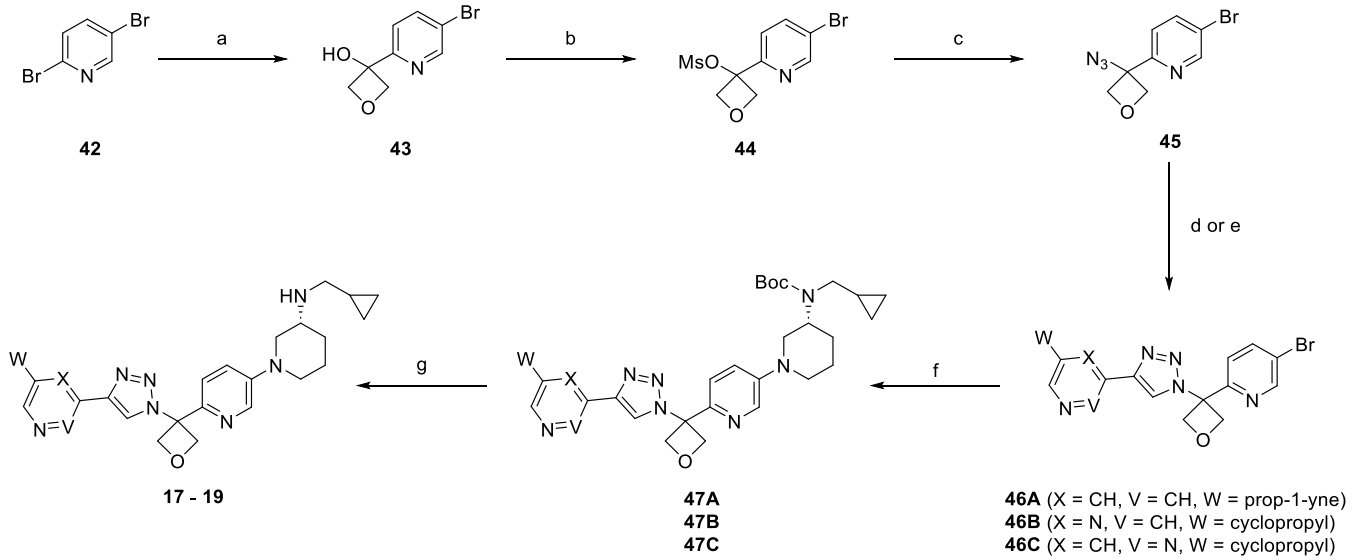

[a]Reagents and conditions: (a) *n*BuLi, 3-oxetanone, Toluene, −78 °C to rt, 1 h, 69%; (b) MsCl, NEt_3, DCM, 0 °C to rt, 1 h, 93%; (c) NaN_3, DMSO, 70 °C, 18 h, 56%; (d) alkyne, CuI, DMF, rt, 16 h, 66−67%; (e) TMS-alkyne, CuF_2, DMF, 60 °C, 32 h, 79%; (f) *tert*-butyl (*R*)-(cyclobutylmethyl)(piperidin-3-yl)carbamate, RuPhos Pd G4, Cs_2CO_3, *t*-AmylOH, 90 °C, 1−17 h, 56−74%; (g) TFA, DCM, rt, 20 min, 63−78%.

https://doi.org/10.1021/acs.jmedchem.6c00474
J. Med. Chem. 2026, 69, 9585−9602

Scheme 4. Preparation of Compound 20[a]

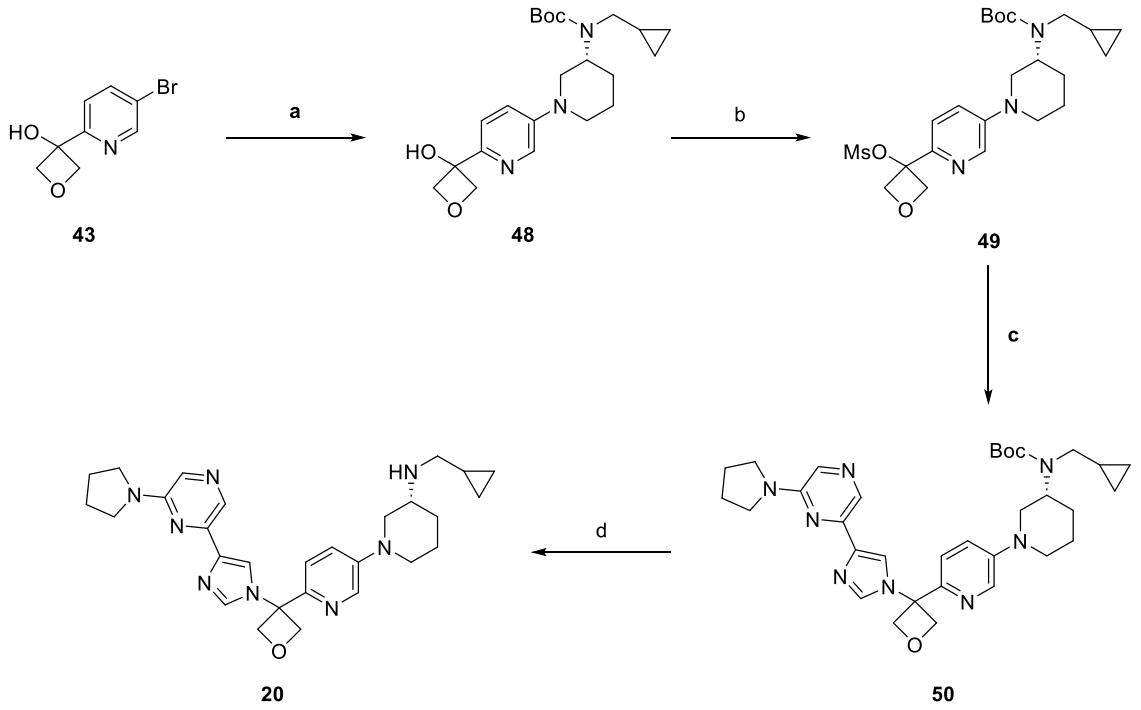

[a]Reagents and conditions: (a) *tert*-butyl (*R*)-(cyclobutylmethyl)(piperidin-3-yl)carbamate, RuPhos Pd G4, Cs_2CO_3, *t*-AmylOH, 120 °C, 90 h, 20%; (b) MsCl, NEt_3, DCM, 0 °C to rt, 1 h, 100%; (c) NaH, 2-(1*H*-imidazol-4-yl)-6-(pyrrolidin-1-yl)pyrazine, DMF, 60 °C, 15 h, 33%; (d) TFA, DCM, rt, 2 h, 25%.

catalyzed reaction with Boc-protected chiral piperidine, delivering intermediates **47** (**A-C**), which were eventually deprotected into compounds **17**−**19**.

For the preparation of compound **20**, the synthetic sequence was inverted from intermediate **43** above. Chiral piperidine was installed first (Scheme 4) and alcohol **48** was then activated into mesylate **49** and attacked mainly at the N-1 nitrogen atom of the substituted imidazole to afford **50** as one of the three detected regioisomers (at the C-2 carbon atom as mentioned in the literature[20] and at the N-3 nitrogen atom in a 5/3/2 ratio). Boc deprotection completed the synthesis of **20**.

Compounds **21** and **22** were prepared from the common oxetane-acid intermediate **55** (Scheme 5). The pathway used started with S_NAr addition of deprotonated cyano-oxetane **51** onto 5-bromo-2-fluoropyridine **52** to afford intermediate **53**. Buchwald−Hartwig cross-coupling then allowed the introduction of the piperidine moiety to obtain cyano-oxetane intermediate **54**. The latter was hydrolyzed to complete access to key acid intermediate **55**. Then, the access to the sequence thiadiazole-oxetane-pyridine was not documented at all, and we had to invest a lot of effort to be able to overcome challenges encountered, such as oxetane susceptibility to opening[21] and difficult thiadiazole formation.[22] An efficient solution was found thanks to T3P: coupling reaction with corresponding thiohydrazide (see Supporting Information) was carried out, followed by *in situ* dehydration to construct the thiadiazole ring of **56**. Assembly of thiadiazole was more difficult than it may appear, as a lot of conditions were attempted. Most activating agents afforded the coupling intermediate from **55** and thiohydrazide; however, consecutive dehydration of the acylated thiohydrazide toward thiadiazole formation was neither efficient with Burgess reagent (from acylated thiohydrazide), Belleau's reagent (from acylated hydrazide), nor using TosylCl.TEA (from acylated thiohydrazide), Lewis acid ($TiCl_4$), or Brønsted acid (TFA) conditions (from acylated thiosemicarbazide). T3P,[23] better described as a condensation agent, was the only efficient reagent found to promote one-pot formation of acylated thiohydrazide intermediate and cyclization/dehydration to form thiadiazole. Standard Boc deprotection of **56** yielded compound **21**. From acid **55**, compound **22** was obtained by a coupling reaction with the desired amino-pyrazine to deliver amide **57**, which was eventually Boc-deprotected.

The medicinal chemistry route toward compound **4** (**EP102**) is shown below in Scheme 6. The pathway used started from the intermediate cyano-oxetane pyridinyl **53** (see Scheme 5). Buchwald−Hartwig cross-coupling allowed the introduction of the piperidine moiety via commercially available (*R*)-3-Boc-aminopiperidine providing **58** without any epimerization. Cyano hydrolysis completed access to our first key intermediate **59**. The second key intermediate thiohydrazide **63** was obtained from **60**: Suzuki cross-coupling to get **61**, which was followed by hydrazine addition, and corresponding hydrazide **62** was then reacted with Lawesson's reagent to afford the desired thiohydrazide **63**. Coupling reaction between **59** and **63** was then carried out, followed by *in situ* dehydration with T3P (*vide supra*) to construct the thiadiazole ring of **64**. Boc deprotection afforded primary amine **65**, which allowed easy access to **EP102** through reductive amination

Process development of the medicinal chemistry route of compound **4** was achieved to successfully provide a scalable GMP route of compound **4** (**EP102**), which delivered a product with excellent purity (99.9% purity and >99.9% enantiomeric excess) in eight steps. Moreover, solid-state characterization and drug product development were also achieved to allow **EP102** nomination as a clinical candidate.

https://doi.org/10.1021/acs.jmedchem.6c00474
J. Med. Chem. 2026, 69, 9585−9602

Scheme 5. Preparation of Compounds 21 and 22[a]

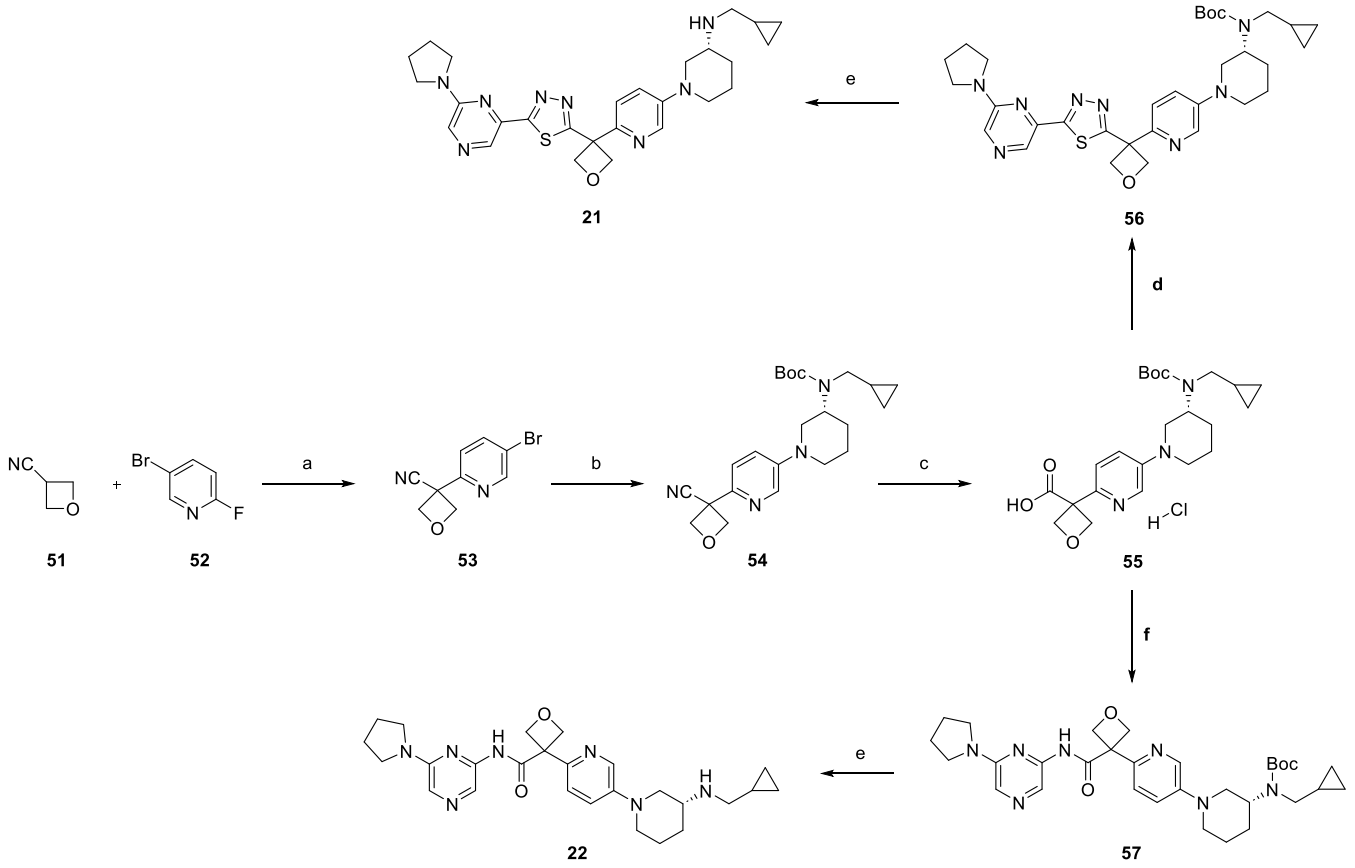

[a]Reagents and conditions: (a) KHMDS, toluene, 0 °C, 40 min, 70%; (b) *tert*-butyl (*R*)-(cyclobutylmethyl)(piperidin-3-yl)carbamate, RuPhos Pd G4, Cs_2CO_3, *t*-AmylOH, 80 °C, 4 h, 80%; (c) NaOH, EtOH, water, 80 °C, 1.5 h, 79%; (d) 6-(pyrrolidin-1-yl)pyrazine-2-carbothiohydrazide, T3P, NEt_3, EtOAc, 55 °C, 10 h, 42%; (e) TFA, DCM, rt, 1 h, 74−89%; (f) 6-(pyrrolidin-1-yl)pyrazin-2-amine, HATU, DIPEA, DMF, 45 °C, 2 h, 69%.

Oxadiazole analogue **23** was obtained *via* a very similar route (Scheme 7). Acid **59** and hydrazide **62** were coupled using HATU, and the corresponding dihydrazide **66** was then dehydrated with Burgess reagent to deliver the desired oxadiazole **67**. Following the same sequence as compound **4**, this intermediate was deprotected with TFA and **68** was then alkylated through reductive amination to provide compound **23**.

CONCLUSIONS

From our proof-of-concept compound **2**, used successfully in several cancer models in mouse despite its limitation of parenteral dosing,[4] the aim of the current work was to elaborate this scaffold to deliver an orally bioavailable METTL3 inhibitor with an appropriate profile for continued development. This phase of lead optimization was initiated from a poorly potent prototype compound (**5**) that nonetheless offered a superior starting point in terms of ADME and oral PK parameters relative to the proof-of-concept compound **2**. Extensive synthetic chemistry efforts permitted the introduction of an oxetane between the triazole hinge and pyridin-3-yl core to afford very interesting compounds such as **9**, being both more potent and, above all, orally available with high unbound exposure in rat. A further boost in potency and improvement of oral unbound AUC was obtained via substitution of the 5-cyclopropylpyridin-3-yl moiety at the left-hand side of the molecule, providing compound **3**. The latter was successfully used as an oral proof-of-concept compound in a mouse model of AML. A final, important modification was the replacement of the triazole of compound **3** with the thiadiazole in compound **4**. The latter change improved compound potency and also enhanced oral rat PK (unbound AUC and bioavailability), and furthermore, this implementation of the thiadiazole is anticipated to be advantageous toward facilitating development of the scale-up manufacturing route by removing the need to deal with the azide.

Development candidate **4** (called **EP102**) has demonstrated profound target engagement *in vivo* by potently inhibiting m^6A in blood samples after a single oral dose in rat. **EP102** also has a promising ADME and selectivity profile, as well as oral bioavailability amenable to repeated dosing across species. **EP102** monotherapy was effective in *in vivo* mouse cancer models of AML and ovarian solid tumors by oral dosing. **EP102** has been advanced into clinical development for the treatment of solid tumors (EUCT number: 205-521305-40-00; NCT07163325).

EXPERIMENTAL SECTION

General Information

All reactions were performed under an argon atmosphere at rt using anhydrous grade solvents, except as otherwise noted. All reagents were used as supplied by the vendor, except as noted. Analytical thin-layer chromatography (TLC) was performed on a Merck silica gel 60 (230−400 mesh). NMR spectra were recorded on a Bruker ARX spectrometer (300 MHz) at rt. Coupling constants (J) are expressed in hertz (Hz). Chemical shifts (δ) are expressed in parts per million relative to the

https://doi.org/10.1021/acs.jmedchem.6c00474
J. Med. Chem. 2026, 69, 9585−9602

Scheme 6. EP102 Medicinal Chemistry Route[a]

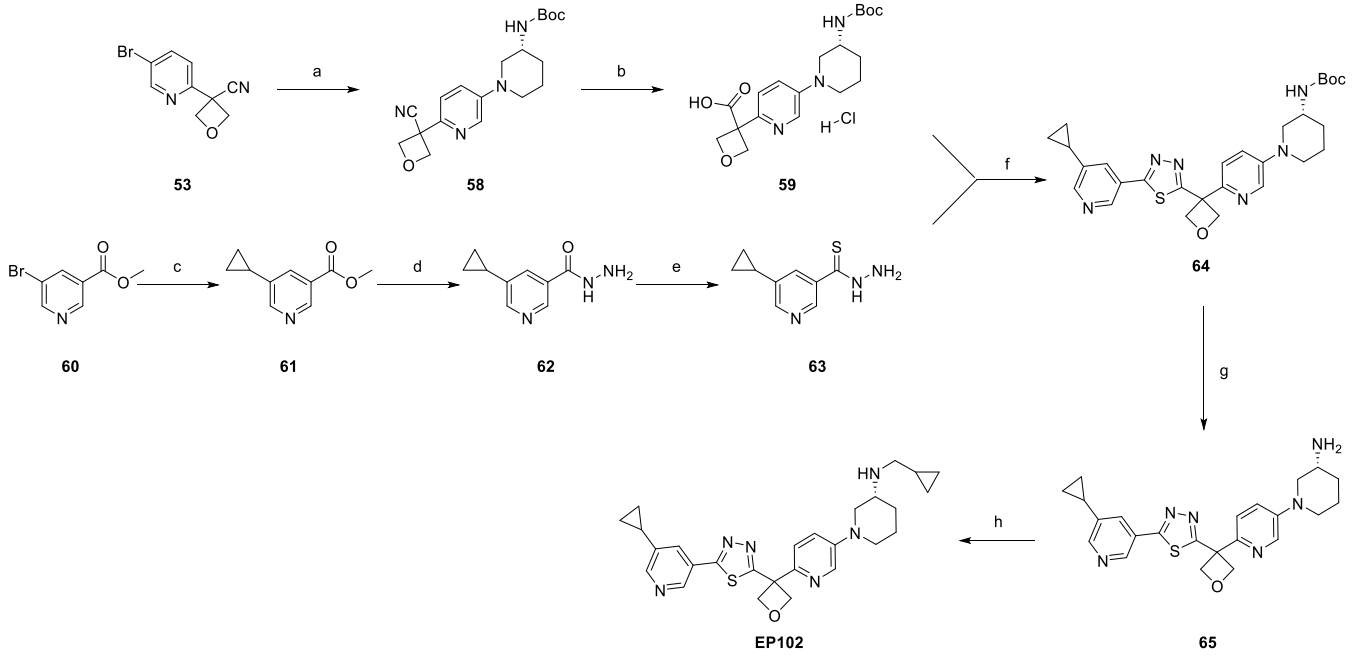

[a]Reagents and conditions: (a) (*R*)-3-Boc-aminopiperidine, RuPhos Pd G4, Cs_2CO_3, *t*-AmylOH, 90 °C, 1.5 h, 90%; (b) NaOH, EtOH, water, 80 °C, 3 h, 84%; (c) *c*PrB$(OH)_2$, Pd$(OAc)_2$, PCy_3, K_3PO_4, toluene, water, 100 °C, 1 h, 88%; (d) $NH_2NH_2.H_2O$, EtOH, 70 °C, 0.5 h, 96%; (e) Lawesson's reagent, 1,4-dioxane, 110 °C, 5 h, 50%; (f) T3P, Et_3N, EtOAc, rt to 40 °C, 3 h, 30%; (g) TFA, DCM, rt, 1.5 h, 80%; (h) *c*PrCHO, $NaBH_4$, AcOH, MeOH, rt, 4.5 h, 79%.

Scheme 7. Preparation of Compound 23[a]

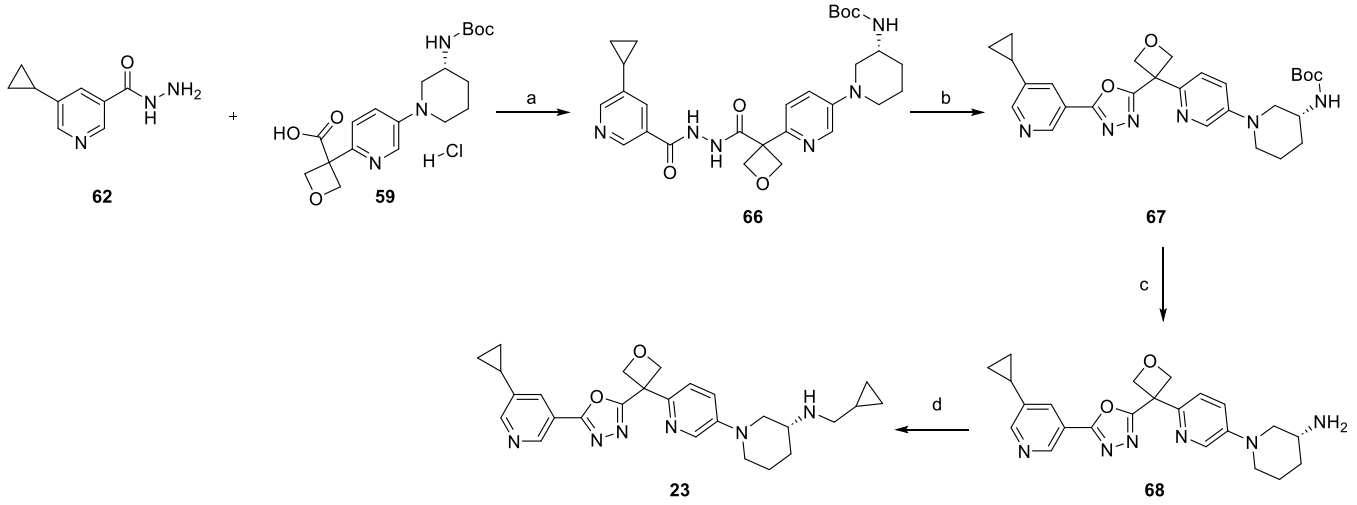

[a]Reagents and conditions: (a) HATU, DIEA, DMF, rt, 10 min, 89%; (b) Burgess reagent, THF, rt, 20 min, 60%; (c) TFA, DCM, rt, 1 h, 78%; (d) *c*PrCHO, $NaBH_3CN$, AcOH, MeOH, rt, 1.5 h, 83%.

residual solvent as an internal reference. Peak multiplicities are expressed as follows: singlet (s), doublet (d), triplet (t), quartet (q), pentaplet (p), hexaplet (h), heptaplet (hept), multiplet (m), and broad singlet (bs). HPLC purity analysis was carried out using one of the following methods. Method A: LC/multiwavelength detector coupled to single quadrupole mass spectrometry detector (LC/UV/MS); column: Sunfire C18 3.5 μm 3.0 × 50 mm; mobile phase A: 0.1% TFA in water (v/v); mobile phase B: 0.1% TFA in CH_3CN (v/v); gradient begins at 5% B, hold 0.2 min at 5% B, increasing to 95% B over 6.0 min, hold at 95% B until 7.75 min; flow rate: 1.0 mL/min. Method B: LC/multiwavelength detector coupled to single quadrupole mass spectrometry detector (LC/UV/MS); column: Sunfire C18 3.5 μm 3.0 × 50 mm; mobile phase A: 0.1% TFA in water (v/v); mobile phase B: 0.1% TFA in CH_3CN (v/v); gradient begins at 5% B, hold 0.2 min at 5% B, increasing to 95% B over 1.8 min, hold at 95% B until 3.75 min; flow rate: 1.0 mL/min. All final compounds are ≥ 95% pure by HPLC analysis or ^{1}H NMR when HPLC was not appropriate. PerkinElmer ChemDraw Professional software (version 22) was used for naming the compounds described below.

3-(5-Bromopyridin-2-yl)oxetane-3-carbonitrile (53) (the Following Procedure Has Been Adapted from *ACS Medicinal Chemistry Letters* 2020, 11, 4, 550−557). To an oven-dried Schlenk tube were added oxetane-3-carbonitrile **51** (2.47 g, 28.24 mmol), 5-bromo-2-fluoropyridine **52** (4.40 g, 24.5 mmol), and anhydrous toluene (120 mL). The reaction mixture was then cooled to 0 °C while stirring under argon. Potassium bis(trimethylsilyl)amide in THF

https://doi.org/10.1021/acs.jmedchem.6c00474
J. Med. Chem. 2026, 69, 9585−9602

solution (40 mL, 35.17 mmol) was then added over 5 min, and the reaction mixture was stirred at 0 °C for 40 min. The reaction was quenched by slow addition of MeOH (25 mL), and the resulting mixture was concentrated under reduced pressure. The crude material was purified by an automated flash chromatography system (0 to 40% EtOAc in heptane) to afford **53** (4.21 g, 70% yield, 98% purity (method B)) as a white solid. m/z (ES^+): $[M + H]^+ = 239, 241$. ^1H NMR (300 MHz, $CDCl_3$) δ 8.79 (dd, J = 2.4, 0.8 Hz, 1H), 7.91 (dd, J = 8.3, 2.4 Hz, 1H), 7.52 (dd, J = 8.3, 0.8 Hz, 1H), 5.19 (d, J = 5.8 Hz, 2H), 5.11 (d, J = 5.9 Hz, 2H). ^{13}C NMR (75 MHz, $CDCl_3$) δ: 152.6, 151.6, 140.1, 122.3, 121.1, 119.9, 79.2, 42.4. TLC (hept/EtOAc, 7/3, v/v, UV 254 nm): $R_f \sim 0.45$.

***tert*-Butyl (*R*)-(1-(6-(3-cyanooxetan-3-yl)pyridin-3-yl)-piperidin-3-yl)carbamate (58).** To an RBF containing (*R*)-3-Boc-aminopiperidine (2.18 g, 10.56 mmol), Cs_2CO_3 (7.70 g, 23.02 mmol), **53** (2.18 g, 8.85 mmol), and RuPhos Pd G4 (742 mg, 0.86 mmol) was evacuated and backfilled with argon (3x). Anhydrous and degassed *tert*-amyl alcohol (30 mL) was added under argon. The reaction mixture was heated at 90 °C for 1.5 h. The reaction mixture was cooled to room temperature, diluted with EtOAc/MeOH (30 mL, 1/1), and filtered through a pad of Celite. The Celite was rinsed with EtOAc/MeOH (150 mL, 1/1). The filtrate was concentrated *in vacuo* to afford a red solid. The crude material was purified by an automated flash chromatography system (0 to 4% MeOH in DCM) to afford **58** (2.95 g, 90% yield, 97% purity (^1H NMR)) as a light-yellow solid. m/z (ES^+): $[M + H]^+ = 359$. ^1H NMR (300 MHz, $CDCl_3$) δ 8.38 (d, J = 2.9 Hz, 1H), 7.41 (dd, J = 8.6, 0.7 Hz, 1H), 7.23 (dd, J = 8.7, 3.1 Hz, 1H), 5.17−5.07 (m, 4H), 4.70 (bs, 1H), 3.81 (bs, 1H), 3.58 (dd, J = 12.1, 3.6 Hz, 1H), 3.41−3.28 (m, 1H), 3.19−3.06 (m, 1H), 2.95 (dd, J = 12.2, 7.6 Hz, 1H), 2.00−1.64 (m, 4H), 1.47 (s, 10H). TLC (DCM/MeOH, 95/5, v/v, UV 254 nm): $R_f \sim 0.65$.

(*R*)-3-(5-(3-((tert-Butoxycarbonyl)amino)piperidin-1-yl)-pyridin-2-yl)oxetane-3-carboxylic Acid.HCl (59). A solution of sodium hydroxide (1.63 g, 40.34 mmol) in water (26 mL) was added to a solution of **58** (2.93 g, 7.85 mmol) in ethanol (26 mL). The reaction mixture was heated to 80 °C for 3 h. The reaction mixture was cooled to room temperature and concentrated under reduced pressure. The oily residue was diluted in water (50 mL) and acidified to pH ∼ 2 with 1 M HCl (40 mL). Acidic solution was extracted with EtOAc (5 × 100 mL). The organic layers were merged, dried over $MgSO_4$, filtered, and concentrated under reduced pressure to afford **59** (3.15 g, 84% yield, 87% purity (^1H NMR)) as an orange foam. m/z (ES^+): $[M + H]^+ = 378$. ^1H NMR (300 MHz, $CDCl_3$) δ 9.74 (bs, 2H), 8.13 (d, J = 3.0 Hz, 1H), 7.80 (d, J = 8.9 Hz, 1H), 7.47 (dd, J = 8.9, 3.0 Hz, 1H), 5.39 (dd, J = 5.9, 1.0 Hz, 2H), 4.73 (dd, J = 5.9, 1.8 Hz, 3H), 3.78 (bs, 1H), 3.64 (dd, J = 12.3, 3.5 Hz, 1H), 3.39 (dd, J = 12.6, 5.5 Hz, 1H), 3.18−3.03 (m, 1H), 2.95 (dd, J = 12.3, 7.8 Hz, 1H), 1.99−1.66 (m, 3H), 1.61−1.39 (m, 10H).

Methyl 5-Cyclopropylnicotinate (61). A Schlenk tube was charged with methyl 5-bromopyridine-3-carboxylate **60** (1.64 g, 7.14 mmol), toluene (36 mL), and water (4 mL), followed by cyclopropylboronic acid (955 mg, 11.12 mmol) and K_3PO_4 (4.83 g, 22.3 mmol). The reaction was bubbled with argon for 10 min. Palladium(II) acetate (95 mg, 0.41 mmol) and tricyclohexylphosphine (240 mg, 0.81 mmol) were added. The tube was closed, and the reaction was heated at 100 °C for 1 h. The reaction mixture was cooled to room temperature, diluted with water (100 mL), and extracted with EtOAc (3 × 100 mL). The organic layer was washed with water (150 mL), brine (150 mL), dried over $MgSO_4$, filtered, and concentrated under reduced pressure. The crude material was purified by an automated flash chromatography system (0 to 50% EtOAc in heptane) to afford **61** (1.14 g, 88% yield, 98% purity (^1H NMR)) as a light-yellow oil. m/z (ES^+): $[M + H]^+ = 178$. ^1H NMR (300 MHz, $CDCl_3$) δ 8.98 (d, J = 2.0 Hz, 1H), 8.58 (d, J = 2.3 Hz, 1H), 7.88 (t, J = 2.2 Hz, 1H), 3.93 (s, 3H), 2.03−1.88 (m, 1H), 1.15−0.99 (m, 2H), 0.83−0.72 (m, 2H). ^{13}C NMR (75 MHz, $CDCl_3$) δ: 166.2, 152.4, 148.1, 139.6, 133.5, 125.8, 52.5, 13.0, 9.4.

5-Cyclopropylnicotinohydrazide (62). To a stirred solution of **61** (570 mg, 3.15 mmol) in anhydrous ethanol (6.3 mL) was added hydrazine monohydrate (1.60 mL, 32.32 mmol). The reaction mixture was stirred at 70 °C for 0.5 h. The reaction mixture was cooled to room temperature and concentrated under reduced pressure to afford **62** (550 mg, 96% yield, 98% purity (method B)) as a gray solid. m/z (ES^+): $[M + H]^+ = 178$. ^1H NMR (300 MHz, DMSO-d_6) δ 9.85 (bs, 1H), 8.73 (d, J = 2.1 Hz, 1H), 8.53 (d, J = 2.3 Hz, 1H), 7.72 (t, J = 2.2 Hz, 1H), 4.52 (bs, 2H), 2.08−1.93 (m, 1H), 1.09−0.97 (m, 2H), 0.85−0.74 (m, 2H). ^{13}C NMR (75 MHz, DMSO-d_6) δ: 164.4, 150.0, 145.3, 139.1, 130.1, 128.5, 12.5, 9.6.

5-Cyclopropylpyridine-3-carbothiohydrazide (63). To a pressure tube under argon were added Lawesson's reagent (3.50 g, 8.48 mmol), **62** (570 mg, 3.15 mmol), and anhydrous 1,4-dioxane (6 mL). The tube was sealed and heated to 110 °C for 5 h. The reaction mixture was cooled to room temperature, and 1,4-dioxane (20 mL) was added. The suspension was filtered. Solid was rinsed off with 1,4-dioxane (2 × 20 mL). Filtrate was concentrated under reduced pressure. The crude material was purified by an automated flash chromatography system (0 to 10% MeOH in DCM) to afford **63** (388 mg, 50% yield, 78% purity (method B + ^1H NMR)) as a yellow solid. m/z (ES^+): $[M + H]^+ = 194$. ^1H NMR (300 MHz, DMSO-d_6) δ 12.23 (bs, 1H), 8.65 (s, 1H), 8.44 (s, 1H), 7.62 (s, 1H), 6.35 (bs, 2H), 2.00 (s, 1H), 1.07−0.96 (m, 2H), 0.83−0.74 (m, 2H). ^{13}C NMR (75 MHz, DMSO-d_6) δ: 178.7, 148.4, 145.1, 138.3, 134.4, 130.2, 12.4, 9.2. TLC (DCM/MeOH, 9/1, v/v, UV 254 nm): Rf ∼ 0.60.

***tert*-Butyl (*R*)-(1-(6-(3-(5-(5-cyclopropylpyridin-3-yl)-1,3,4-thiadiazol-2-yl)oxetan-3-yl)pyridin-3-yl)piperidin-3-yl)-carbamate (64).** To a stirred solution of **63** (84 mg, 0.34 mmol) and **59** (178 mg, 0.37 mmol) in anhydrous EtOAc (1.7 mL) under argon at room temperature were added triethylamine (150 μL, 1.08 mmol) and then T3P (in EtOAc, 50 wt % solution) (280 μL, 0.47 mmol). The suspension was stirred at room temperature for 2 h and then heated at 40 °C for 30 min. A second addition of T3P (in EtOAc, 50 wt % solution) (280 μL, 0.47 mmol) was carried out, and the reaction mixture was heated at 40 °C for 20 min. Reaction mixture was cooled to room temperature, diluted with EtOAc (50 mL) and washed with a saturated aqueous solution of $NaHCO_3$ (2 × 20 mL), brine (25 mL), dried over $MgSO_4$, filtered, and concentrated under reduced pressure to give a brown solid. The crude material was purified by an automated flash chromatography system (0 to 3% MeOH in DCM) to afford **64** (74 mg, 30% yield, 74% purity (^1H NMR)) as a colorless oil. m/z (ES^+): $[M + H]^+ = 535$. ^1H NMR (300 MHz, $CDCl_3$) δ 8.82 (d, J = 1.9 Hz, 1H), 8.50 (d, J = 2.0 Hz, 1H), 8.33 (s, 1H), 7.90 (s, 1H), 7.25−7.19 (m, 2H), 5.48 (dd, J = 5.8, 1.8 Hz, 2H), 5.36 (d, J = 5.9 Hz, 2H), 4.73 (s, 1H), 3.82 (s, 1H), 3.61−3.50 (m, 1H), 3.40−3.27 (m, 1H), 3.17−3.05 (m, 1H), 3.02−2.91 (m, 1H), 2.00−1.69 (m, 4H), 1.56−1.43 (m, 10H), 1.16−1.03 (m, 2H), 0.86−0.75 (m, 2H). ^{13}C NMR (75 MHz, $CDCl_3$) δ: 173.2, 166.7, 155.0, 150.3, 149.6, 146.0, 145.5, 139.9, 137.9, 130.7, 125.8, 123.4, 120.8, 80.6, 79.1, 53.9, 50.7, 48.5, 46.0, 29.7, 28.2, 22.5, 12.7, 9.3, 1.6.

(*R*)-1-(6-(3-(5-(5-Cyclopropylpyridin-3-yl)-1,3,4-thiadiazol-2-yl)oxetan-3-yl)pyridin-3-yl)piperidin-3-amine (65). To a solution of **64** (74 mg, 0.1 mmol) in anhydrous DCM (1.0 mL) under an Ar atmosphere was added TFA (170 μL, 2.18 mmol). The reaction mixture was stirred at room temperature for 1.5 h. Then, the reaction mixture was diluted with a saturated aqueous solution of $NaHCO_3$ (10 mL) and extracted with DCM (3 × 30 mL). The combined organic layers were dried over $MgSO_4$, filtered, and concentrated under reduced pressure to dryness to afford a yellow oil. The crude product was purified by reversed-phase preparative HPLC (Waters XBridge OBD C18 5 μm, 19 mm × 100 mm, mobile phase: "A" = ammonium bicarbonate 0.01 M (pH = 8); "B" = MeCN. Gradient used: increased linearly from 25 to 45% of "B" over 4.5 min, increased linearly from 45 to 88% of "B" over 1.5 min, held at 88% during 1.5 min, returned to initial conditions over 0.7 min, 15 mL/min), affording **65** (36 mg, 81% yield, 100% (method B)) as a pale-yellow oil. m/z (ES^+): $[M + H]^+ = 435$. ^1H NMR (300 MHz, $CDCl_3$) δ 8.80 (d, J = 2.1 Hz, 1H), 8.49 (d, J = 2.2 Hz, 1H), 8.33 (t, J = 1.9 Hz, 1H), 7.88 (t, J = 2.2 Hz, 1H), 7.22 (s, 1H), 7.21 (s, 1H), 5.48 (d, J = 5.9 Hz, 2H), 5.36 (d, J = 5.9 Hz, 2H), 3.65−3.55 (m, 1H), 3.55−3.44 (m, 1H), 3.06−2.94 (m, 1H), 2.93−2.82 (m, 1H), 2.65 (dd, J = 11.9, 8.9 Hz, 1H), 2.03−1.80 (m, 3H), 1.78−1.55 (m, 3H), 1.38−1.27 (m, 1H), 1.14−1.05 (m, 2H), 0.86−0.74 (m, 2H). ^{13}C NMR (75 MHz, $CDCl_3$) δ: 173.6, 167.0, 150.7,

https://doi.org/10.1021/acs.jmedchem.6c00474
J. Med. Chem. 2026, 69, 9585−9602

149.9, 146.5, 146.0, 140.3, 138.2, 131.0, 126.2, 123.6, 121.1, 81.0, 57.5, 51.1, 48.7, 47.6, 33.8, 23.4, 13.1, 9.6.

(*R*)-N-(Cyclopropylmethyl)-1-(6-(3-(5-(5-cyclopropylpyridin-3-yl)-1,3,4-thiadiazol-2-yl)oxetan-3-yl)pyridin-3-yl)piperidin-3-amine EP102 (4). A solution of **65** (36 mg, 0.08 mmol) and cyclopropanecarboxaldehyde (8 μL, 0.1 mmol) in anhydrous methanol (1.4 mL) under Ar atmosphere was treated with acetic acid (5 μL, 0.09 mmol). After 10 min of stirring at room temperature, sodium cyanoborohydride (17 mg, 0.26 mmol) was added, and the resulting mixture was stirred for 4.5 h. The reaction was quenched with saturated aqueous solution of $NaHCO_3$ (15 mL) and extracted with DCM (3 × 20 mL). The organic layer was dried over $MgSO_4$, filtered, and concentrated under reduced pressure to afford a colorless oil. The product was purified by reversed-phase preparative HPLC (XBridge OBD C18 5 μm, 19 × 100 mm. Gradient used: increased linearly from 40% to 45% solution "B" over 6.0 min, increased linearly to 50% solution "B" over 1.0 min, increased linearly to 88% of "B" over 2.5 min, held to 88% for 1.5 min, and returned to initial conditions over 1.5 min. Flow Rate: 18 mL/min), affording **4** (**EP102**) (30 mg, 75% yield, 100% purity (method A)) as a yellow oil. Chiral HPLC (IA, TBME/MeOH/DCM/DEA, 40/40/20/0.1) purity at 280 nm = 100%, ee >99.9%. *m*/*z* (ES^+): $[M + H]^+$ = 489. ^1H NMR (300 MHz, $CDCl_3$) δ 8.80 (d, J = 2.2 Hz, 1H), 8.49 (d, J = 2.3 Hz, 1H), 8.32 (d, J = 2.2 Hz, 1H), 7.88 (t, J = 2.2 Hz, 1H), 7.22 (s, 2H), 5.46 (d, J = 6.0 Hz, 2H), 5.35 (d, J = 5.9 Hz, 2H), 3.72−3.62 (m, 1H), 3.55−3.43 (m, 1H), 3.02−2.82 (m, 1H), 2.82−2.64 (m, 2H), 2.63−2.44 (m, 2H), 2.02−1.88 (m, 2H), 1.87−1.76 (m, 1H), 1.76−1.57 (m, 1H), 1.53−1.21 (m, 2H), 1.15−1.01 (m, 2H), 1.00−0.89 (m, 1H), 0.85−0.73 (m, 2H), 0.55−0.43 (m, 2H), 0.17−0.06 (m, 2H). ^{13}C NMR (75 MHz, $CDCl_3$) δ: 173.3, 166.6, 150.3, 149.3, 146.2, 145.6, 139.8, 137.7, 130.7, 125.8, 123.0, 120.7, 80.6, 54.5, 53.2, 52.1, 50.8, 48.7, 30.7, 23.0, 12.7, 11.4, 9.2, 3.2. HRMS (ESI-TOF) *m*/*z*: calcd for $C_{27}H_{36}N_7OS$ $[M+NH_4]^+$ = 506.2697, found 506.2788.

■ ASSOCIATED CONTENT

Supporting Information

The Supporting Information is available free of charge at https://pubs.acs.org/doi/10.1021/acs.jmedchem.6c00474.

Molecular formula strings table (CSV)

Experimental data, including experimental procedures for all compounds and NMR spectra; SPA, ATPlite and intracellular m^6A assays; plasma protein binding determination, cytotoxicity assay, metabolic stability, cytochrome P450 inhibition, hERG assay; methyltransferase selectivity assay; safety screen panel; plasma pharmacokinetic studies in rats, mice and minipigs; biomarkers evaluation; full description of *in vivo* cancer models; method for LogD determination; and cocrystallization details: protein production, crystallization of apo complex and tabulated parameters of data collection and structure refinement for compounds **3**, **4** (**EP102**), **8**, and **13** (PDF)

Accession Codes

Crystallographic structures of compounds **3**, **8**, **13**, and **4** (**EP102**) complexed to truncated METTL3/14 proteins have been deposited at the Protein Data Bank with the accession codes 9Q8A, 9IH5, 9Q89, and 9Q8G, respectively. The authors will release the atomic coordinates and experimental data upon article publication.

■ AUTHOR INFORMATION

Corresponding Author

Guillaume Dutheuil − *Epics Therapeutics SA, 6041 Gosselies, Belgium;* orcid.org/0000-0002-8887-4823; Email: gdutheuil@epicstx.com

Authors

Killian Oukoloff − *Epics Therapeutics SA, 6041 Gosselies, Belgium*

François Lenoir − *Epics Therapeutics SA, 6041 Gosselies, Belgium*

Julien Korac − *Epics Therapeutics SA, 6041 Gosselies, Belgium*

Mohamed El Bousmaqui − *Epics Therapeutics SA, 6041 Gosselies, Belgium*

Nicolas Probst − *Epics Therapeutics SA, 6041 Gosselies, Belgium;* orcid.org/0000-0003-1941-7132

Alexey Lapin − *Epics Therapeutics SA, 6041 Gosselies, Belgium*

Galina Nakhabina − *Epics Therapeutics SA, 6041 Gosselies, Belgium*

Nicolas Parmentier − *Epics Therapeutics SA, 6041 Gosselies, Belgium;* orcid.org/0000-0002-9114-3976

Catherine Sorlet − *Epics Therapeutics SA, 6041 Gosselies, Belgium*

Graeme L. Fraser − *Epics Therapeutics SA, 6041 Gosselies, Belgium*

Complete contact information is available at: https://pubs.acs.org/10.1021/acs.jmedchem.6c00474

Author Contributions

The manuscript was written through contributions of all authors. All authors have given approval to the final version of the manuscript.

Funding

The work was mainly funded by Epics Therapeutics. This research project was partially supported by a research grant from the Walloon Region, Belgium.

Notes

The authors are all employees of EPICS Therapeutics. All animal experiments performed in the manuscript were conducted in compliance with institutional guidelines. All rat and mouse experiments were performed following the protocols evaluated and approved (approval number 271-2025) by the Animal well-being Ethics Committee (CEBEA) and affiliation (facility authorization CEBEA 271-2025). The minipig experimental study protocol was sent to the competent authorities (DTES: Departament de Territori I Sostenibilitat de la Generalitat de Catalunya) and approved (Specific Pig S.L B9900041). All procedures carried out in the MV-4-11 experiment were conducted in compliance with the applicable laws, regulations, and guidelines of the National Institutes of Health (NIH) and with the approval of Labcorp PCO's Animal Care and Use Committee. Labcorp (Ann Arbor) is an AAALAC-accredited facility. The SK-OV-3 study was performed according to the protocol approved by the Institutional Animal Care and Use Committee (IACUC) of Shanghai ChemPartner following the guidance of the Association for Assessment and Accreditation of Laboratory Animal Care (AAALAC).

The authors declare no competing financial interest.

■ ACKNOWLEDGMENTS

We thank our colleagues in the *in vitro* and *in vivo* profiling teams as well as the pharmacology team for conducting studies in support of this work. The early contributions of Dr. Karila and her team at Paraza Pharma, Montreal, Quebec, Canada, are gratefully acknowledged. We are grateful as well to Dr. Dawidowski and his team at Selvita, Krakow, Poland, for the

determination of X-ray structures of truncated human METTL3/14 complex with our compounds. Finally, we are grateful to Dr. Slater and his team at Cresset Discovery, UK, for the exceptional modeling work conducted to initiate the discoveries described herein,[24] and to Maciej Dabrowski at Gordion Bioscience for the gene amplification analysis highlighting the coamplification of METTL3 and PARP2.

■ ABBREVIATIONS USED

ADME, absorption, distribution, metabolism, and excretion; ADMP, 2-azido-1,3-dimethylimidazolinium hexafluorophosphate; AML, acute myeloid leukemia; ATP, adenosine triphosphate; AUC, aera under the curve; BLI, bioluminescence imaging; Boc, *tert*-butyloxycarbonyl; calcd, calculated; CDX, cell line-derived xenograft; conc, concentration; cy, cyclohexyl; CYP, cytochrome P450; DBU, 1,8-Diazabicyclo[5.4.0]undec-7-ene; DCM, dichloromethane; DEA, diethylamine; DIPEA, diisopropylethylamine; DMF, dimethylformamide; DMSO, dimethyl sulfoxide; DPPA, diphenyl phosphoryl azide; EtOH, ethanol; FACS, Fluorescence Activated Cell Sorting; FTO, fat-mass and obesity-associated gene; GLP, good laboratory practice; GMP, good manufacturing practice; GPCR, G-protein coupling receptors; HPLC, high-performance liquid chromatography; IC_{50}, half-maximum inhibitory concentration; HATU, hexafluorophosphate azabenzotriazole tetramethyl uronium; hept, heptane; hERG, human ether-a-go-go related gene; HLM, human liver microsomes; *ip*, intraperitoneal administration; *iv*, intravenous administration; KHMDS, potassium hexamethyldisilazane; LLE, ligand lipophilic efficiency; LHS, left-hand side; MeOH, methanol; METTL3, methyltransferase-like 3; MpLM, minipig liver microsomes; MsCl, mesityl chloride; NMR, nuclear magnetic resonance; NMP, *N*-methylpyrrolidine; NSG mice, NOD scid γ mice; PK, pharmacokinetic; *po*, oral administration; PoC, proof-of-concept; PPB, plasma proteins binding; QD, quaque die (once a day); QSAR, quantitative structure−activity relationship; RBF, round-bottom flask; rfu, rat free unbound fraction (PPB); RHS, right-hand side; RLM, rat liver microsomes; RNA, ribonucleic acid; rt, room temperature; SAR, structure−activity relationship; SNAr, Aromatic Nucleophilic Substitution; SPA, scintillation proximity assay; T3P, propylphosphonic anhydride; TBME, *tert*-butyl methyl ether; TFA, trifluoroacetic acid; TGI, tumor growth inhibition; THF, tetrahydrofuran; TIW, three times a week; TLC, thin-layer chromatography

■ REFERENCES

(1) (a) Garcias Morales, D.; Reyes, J. L. A birds'-eye view of the activity and specificity of the mRNA m6A methyltransferase complex. *Wiley Interdiscip Rev. RNA* **2021**, *12*, No. e1618. (b) Knuckles, P.; Lence, T.; Haussmann, I. U.; Jacob, D.; Kreim, N.; Carl, S. H.; Masiello, I.; Hares, T.; Villaseñor, R.; Hess, D.; Andrade-Navarro, M. A.; Biggiogera, M.; Helm, M.; Soller, M.; Bühler, M.; Roignant, J.-Y. Zc3h13/Flacc is required for adenosine methylation by bridging the mRNA-binding factor Rbm15/Spenito to the m6A machinery component Wtap/Fl(2)d. *Genes Dev.* **2018**, *32*, 415−429.

(2) (a) Jin, Q.; Qu, H.; Quand, C. New insights into the regulation of METTL3 and its role in tumors. *Cell Commun. Signal.* **2023**, *21*, No. 334. (b) Wu, Z.; Smith, A. R.; Qian, Z.; Zheng, G. Patent landscape of small molecule inhibitors of METTL3 (2020-present). *Expert Opin. Ther. Pat.* **2025**, *35*, 1−16.

(3) (a) Moroz-Omori, E. V.; Huang, D.; Bedi, R. K.; Cheriyamkunnel, S. J.; Bochenkova, E.; Dolbois, A.; Rzeczkowski, M. D.; Li, Y.; Wiedmer, L.; Caflisch, A. METTL3 inhibitors for epitranscriptomic modulation of cellular processes. *ChemMedChem* **2021**, *16*, 3035−3043. (b) Yankova, E.; Blackaby, W.; Albertella, M.; Rak, J.; De Braekeleer, E.; Tsagkogeorga, E.; Pilka, E. S.; Aspris, D.; Leggate, D.; Hendrick, A. G.; Webster, N. A.; Andrews, B.; Fosbeary, R.; Guest, P.; Irigoyen, N.; Eleftheriou, M.; Gozdecka, M.; Dias, J. M. L.; Bannister, A. J.; Vick, B.; Jeremias, I.; Vassiliou, G. S.; Rausch, O.; Tzelepis, K.; Kouzarides, K. Small molecule inhibition of METTL3 as a strategy against myeloid leukaemia. *Nature* **2021**, *593*, 597−601.

(4) (a) Dutheuil, G.; Oukoloff, K.; Korac, J.; Lenoir, F.; El Bousmaqui, M.; Probst, N.; Lapin, A.; Nakhabina, G.; Sorlet, C.; Parmentier, N.; Karila, D.; Ghavtadze, N.; Casualt, P.; Claridge, S.; Sapmaz, S.; Slater, M. J.; Fraser, G. L. Discovery, Optimization, and Preclinical Pharmacology of EP652, a METTL3 Inhibitor with Efficacy in Liquid and Solid Tumor Models. *J. Med. Chem.* **2025**, *68* (3), 2981−3003. (b) Dutheuil, G.; Fraser, G.; Sorlet, C.; Oukoloff, K.; Lenoir, F.; Korac, J. Piperidine derivatives as METTL3 inhibitors. WO2024/153775A1, Jul 25, 2024.

(5) (a) Leeson, P. D.; Empfield, J. R. Reducing the risk of drug attrition associated with physicochemical properties. *Annu. Rep. Med. Chem.* **2010**, *45*, 381−391. and references therein (b) Johnson, T. W.; Gallego, R. A.; Edwards, M. P. Lipophilic Efficiency as an Important Metric in Drug Design. *J. Med. Chem.* **2018**, *61*, 6401−6420.

(6) (a) Miller, R. R.; Madeira, M.; Wood, H. B.; Geissler, W. M.; Raab, C. E.; Martin, I. J. Integrating the impact of lipophilicity on potency and pharmacokinetic parameters enables the use of diverse chemical space during small molecule drug optimization. *J. Med. Chem.* **2020**, *63* (21), 12156−12170. (b) Pennington, L. D.; Hesse, M. J.; Koester, D. C.; McAtee, R. C.; Qunies, A. M.; Xu, D. X. Property-Based Drug Design Merits a Nobel Prize. *J. Med. Chem.* **2024**, *67*, 11452−11458.

(7) Recent report on optimization of in vitro metabolic stability of METTL3 inhibitors: Matter, C. M.; Caflisch, A. Fine-tuning a transformer model for METTL3 lead optimization *J. Med. Chem.* 2026 DOI: 10.1021/acsbiomedchemau.5c00198.

(8) (a) Summerfield, S. G.; Yates, J. W. T.; Fairman, D. A. Free drug theory - No longer just a hypothesis? *Pharm. Res.* **2022**, *39* (2), 213−222. (b) Trainor, G. L. The importance of plasma protein binding in drug discovery. *Expert Opin. Drug Discovery* **2007**, *2*, 51−64. and references therein (c) Webborn, P. J. H.; Beaumont, K.; Martin, I. J.; Smith, D. A. Free Drug Concepts: A Lingering Problem in Drug Discovery. *J. Med. Chem.* **2025**, *68* (7), 6850−6856.

(9) Compound **32** in previous report.[4]

(10) (a) Wuitschik, G.; Rogers-Evans, M.; Müller, K.; Fischer, H.; Wagner, B.; Schuler, F.; Polonchuk, L.; Carreira, E. M. Oxetanes as Promising Modules in Drug Discovery. *Angew. Chem., Int. Ed.* **2006**, *45* (46), 7736−7739. (b) Rojas, J. J.; Bull, J. A. Oxetanes in Drug Discovery Campaigns. *J. Med. Chem.* **2023**, *66* (17), 12697−12709. (c) Bull, J. A.; Croft, R. A.; Davis, O. A.; Doran, R.; Morgan, K. F. Oxetanes: Recent Advances in Synthesis, Reactivity, and Medicinal Chemistry. *Chem. Rev.* **2016**, *116* (19), 12150−12233. (d) Recent example of successful introduction of an oxetane: Huff, S.; Kummetha, I. R.; Zhang, L.; Wang, L.; Bray, W.; Yin, J.; Kelley, V.; Wang, Y.; Rana, T. M. Rational Design and Optimization of m^6A-RNA Demethylase FTO Inhibitors as Anticancer Agents. *J. Med. Chem.* **2022**, *65* (16), 10920−10937. (e) Li, D.; Sloman, D. L.; Achab, A.; Zhou, H.; McGowan, M. A.; White, C.; Gibeau, C.; Zhang, H.; Pu, Q.; Bharathan, I.; Hopkins, B.; Liu, K.; Ferguson, H.; Fradera, X.; Lesburg, C. A.; Martinot, T. A.; Qi, J.; Song, Z. J.; Yin, J.; Zhang, H.; Song, L.; Wan, B.; Daddio, S.; Solban, N.; Miller, J. R.; Zamlynny, B.; Bass, A.; Freeland, E.; Ykoruk, B.; Hilliard, C.; Ferraro, J.; Zhai, J.; Knemeyer, I.; Otte, K. M.; Vincent, S.; Sciammetta, N.; Pasternak, A.; Bennett, D. J.; Han, Y. Oxetane Promise Delivered: Discovery of Long-Acting IDO1 Inhibitors Suitable for Q3W Oral or Parenteral Dosing. *J. Med. Chem.* **2022**, *65* (8), 6001−6016.

(11) PDB: 9Q8A, 9IH5 and 9Q89.

(12) Historical data accrued at EPICS from numerous concentration−response experiments (conducted with different METTL3 inhibitors, both *in vitro* and *in vivo*) consistently indicates that the maximal, achievable reduction of m^6A/A is typically in the range of ∼80%, which is corroborated by findings in the literature following CRISPR/Cas9-knockdown of METTL3 Poh, H. X.; Mirza, A. H.;

https://doi.org/10.1021/acs.jmedchem.6c00474
J. Med. Chem. 2026, 69, 9585−9602

Pickering, B. F.; Jaffrey, S. R. Alternative splicing of *METTL3* explains apparently METTL3-independent m^{6}A modifications in mRNA. *PLoS Biol.* **2022**, *20* (7), No. e3001683.
(13) Method: **Whole-Genome Sequencing Data and Copy Number Analysis**. Whole-genome sequencing data were obtained from The Cancer Genome Atlas (TCGA) repository (access granted to Gordion Bioscience) for a total of 553 ovarian cancer cases. For each case, paired tumor and matched-normal samples were analyzed. Sequencing was performed on the Illumina platform with an average coverage depth of approximately 30x. Raw sequencing data were provided as FASTQ files and aligned to the GRCh37.d5 human reference genome using the Burrows−Wheeler Aligner (BWA-MEM) algorithm. Post-alignment processing followed standard best practices. Somatic copy number alterations were identified and analyzed using the ASCAT3 tool, which estimates allele-specific copy number profiles by jointly modeling tumor purity and ploidy based on matched tumor−normal sequencing data.
(14) Kulkarni, S.; Seneviratne, N.; Tosun, ç.; Madhusudan, S. PARP inhibitors in ovarian cancer: Mechanisms of resistance and implications to therapy. *DNA Repair* **2025**, *149*, No. 103830.
(15) Ruiz-Castillo, P.; Buchwald, S. L. Applications of Palladium-Catalyzed C-N Cross-Coupling Reactions. *Chem. Rev.* **2016**, *116* (19), 12564−12649.
(16) Thompson, A. S.; Humphrey, G. R.; DeMarco, A. M.; Mathre, D. J.; Grabowski, E. J. J. Direct conversion of activated alcohols to azides using diphenyl phosphorazidate. A practical alternative to Mitsunobu conditions. *J. Org. Chem.* **1993**, *58* (22), 5886−5888.
(17) Kolb, H. C.; Finn, M. G.; Sharpless, K. B. Click chemistry: diverse chemical function from a few good reactions. *Angew. Chem., Int. Ed* **2001**, *40* (11), 2004−2021.
(18) Kitamura, M.; Kato, S.; Yano, M.; Tashiro, N.; Shiratake, Y.; Sando, M.; Okauchi, T. A reagent for safe and efficient diazo-transfer to primary amines: 2-azido-1, 3-dimethylimidazolinium hexafluorophosphate. *Org. Biomol. Chem.* **2014**, *12*, 4397−4406.
(19) Friscourt, F.; Boons, G. J. One-pot three-step synthesis of 1,2,3-triazoles by copper-catalyzed cycloaddition of azides with alkynes formed by a Sonogashira cross-coupling and desilylation. *Org. Lett.* **2010**, *12* (21), 4936−4939.
(20) Richaud, A.; Barba-Behrens, N.; Méndez, F. Chemical Reactivity of the Imidazole: A Semblance of Pyridine and Pyrrole? *Org. Lett.* **2011**, *13* (5), 972−975.
(21) Ahmad, S.; Yousaf, M.; Mansha, A.; Rasool, N.; Zahoor, A. F.; Hafeez, F.; Rizvi, S. M. A. Ring-opening reactions of oxetanes: A review of methodology development and synthetic applications. *Synth. Commun.* **2016**, *46* (17), 1397−1416.
(22) Hu, Y.; Li, C. Y.; Wang, X. M.; Yang, Y. H.; Zhu, H. L. 1,3,4-Thiadiazole: Synthesis, Reactions, and Applications in Medicinal, Agricultural, and Materials Chemistry. *Chem. Rev.* **2014**, *114*, 5572−5610.
(23) Augustine, J. K.; Vairaperumal, V.; Narasimhan, S.; Alagarsamy, P.; Radhakrishnan, A. Propylphosphonic anhydride (T3P): an efficient reagent for the one-pot synthesis of 1,2,4-oxadiazoles, 1,3,4-oxadiazoles, and 1,3,4-thiadiazoles. *Tetrahedron* **2009**, *65*, 9989−9996.
(24) Slater, M. Accelerating discovery of a METTL3 inhibitor through efficient in silico design and prioritization. https://cresset-group.com/science/science-resources/accelerating-discovery-mettl3-inhibitor-efficient-in-silico-design-and-prioritization/.

https://doi.org/10.1021/acs.jmedchem.6c00474
J. Med. Chem. 2026, 69, 9585−9602